2017

Terahertz Molecular Spectroscopy as a Tool for Analytical Probing of Cellular Metabolism

Mitchell Cameron Paul
Wright State University

TERAHERTZ MOLECULAR SPECTROSCOPY AS A TOOL FOR ANALYTICAL PROBING OF CELLULAR METABOLISM

A thesis submitted in partial fulfillment of the requirements for the degree of Master of Science

By

MITCHELL CAMERON PAUL
B.S. Wright State University, 2016

2017
Wright State University

WRIGHT STATE UNIVERSITY

GRADUATE SCHOOL

August 2, 2017

I HEREBY RECOMMEND THAT THE THESIS PREPARED UNDER MY SUPERVISION BY Mitchell Cameron Paul ENTITLED Terahertz Molecular Spectroscopy as a Tool for Analytical Probing of Cellular Metabolism BE ACCEPTED IN PARTIAL FULFILLMENT OF THE REQUIREMENTS FOR THE DEGREE OF Master of Science.

_____
Ivan R. Medvedev, Ph. D.
Thesis Director

_____
Jason Deibel Ph. D.
Chair, Department of Physics

Committee on
Final Examination

_____
Ivan Medvedev Ph.D.

_____
Jerry Clark, Ph. D.

_____
Jason Deibel Ph. D.

_____
Robert E. W. Fyffe, Ph.D.
Vice President for Research and
Dean of the Graduate School

ABSTRACT

Paul, Mitchell Cameron. M.S. Department of Physics, Wright State University, 2017.
Terahertz Molecular Spectroscopy as a Tool for Analytical Probing of Cellular Metabolism

Terahertz spectroscopy has found use as an analytical tool in determining chemical composition of exhaled human breath. This thesis demonstrates a novel application of this technology - analytical sensing of gaseous metabolic products of several types of human cell cultures. An innovative experimental system was developed for probing cellular metabolism using terahertz [THz] rotational spectroscopy. Gaseous emissions of cell cultures were analyzed and compared between several cell types. Cancerous and healthy lung cells as well as cancerous liver cells were studied. This technique carries a lot of promise as a noninvasive method of distinguishing between cell types and identifying cell pathologies. In this set of experiments, prominent variance in the rates of acetaldehyde metabolism was identified, which can potentially be used as a diagnostic method of cellular identification. Possible applications of this novel technique might extend to the medical field, where it will be used as a non-invasive detection and diagnostic tool.

Table of Contents

List of Figures

List of Tables

Chapter 1

1.1 Introduction

Terahertz rotational spectroscopy as a means of probing cellular metabolism is a novel technique. By monitoring the gaseous emissions of cell cultures, it may be possible to gain insight into the biochemical processes in these cells. For example, comparisons can be made between healthy and cancerous cells in order to identify biomarkers or rates of metabolism present in one and absent in the other. This could be extended to other areas of interest including detection of biomarkers indicative of early-onset diabetes [1] and detection of viral infection. Terahertz rotational spectroscopy has recently emerged as a non-invasive tool in biological investigations. In particular, THz spectroscopy has found use in chemical analysis of exhaled breath, [2] through its speed and relatively low cost, and it will likely be welcomed across many applications. However, human breath analysis is an incredibly complex field of study including many biological processes. For instance, in THz breath analysis, hydrogen cyanide [HCN] is nearly always detected. HCN is thought to be present in human breath due to common bacteria in the mouth and has no relevance to anything occurring in the lungs or other human organs. [3] By studying directly the metabolism of cells in cultures, the thesis investigates a single important piece of the complex puzzle that is THz breath analysis. This study provides a basis for further studies in using THz rotational spectroscopy as an investigative tool in understanding metabolic pathways in various cell culture types.

A discussion of the cell lines and media types used in this research can be found in Chapter 2. In addition, the biological processes relevant to this study are outlined in

Chapter 2. Metabolic pathways for the compounds of interest are discussed as well as the bio-relevance of the associated compounds.

Chapter 3 details the procedures and experiments developed in the course of the study, including the precautions that were taken to ensure consistency and viability of data collected, especially where the cell cultures were involved. For example, collection time, gas flow rate, enclosure temperature, and sample volume were standardized. The THz spectroscopic techniques and methods are also discussed in this chapter.

Chapter 4 presents the results of the experiment. Trends in formaldehyde, methanol, ethanol, acetone, and acetaldehyde are discussed for each cell type. Comparisons are made between observed metabolic rates of acetaldehyde in each cell type. Additional topics discussed include challenges faced, plans for future study, and potential applications of the developed technique.

Chapter 5 entails a discussion on the significant outcomes of the results. Potential for further research is also addressed.

1.2 Terahertz Radiation and Applications of Terahertz Spectroscopy

The terahertz [THz] region of the electromagnetic spectrum, ranging from 0.1 THz to 10 THz, has seen elevated interest and a correlated technological growth over the last several decades. THz radiation is bordered on either side by the infrared and microwave regions and displays some traits of each. Applications of terahertz radiation cover a wide array of disciplines including ultrafast photonics, optics, physical chemistry, and biophysics, and are generally divided into two categories: THz imaging and THz spectroscopy. Many materials that are opaque in the visible spectrum are transparent in the terahertz spectral range. Using unique properties of THz radiation, imaging

applications range from identification and differentiation of powdery substances in unopened envelopes that would otherwise be indistinguishable [4] to nondestructive evaluation of aircraft materials. [5] THz spectroscopy has drawn interest in medical applications and biological research due to its noninvasive and non-ionizing nature, the transparency of nonpolar biological samples in the THz region, and its strong absorption by water. [6] One particular use of these properties is early detection of skin cancer through differentiating healthy and cancerous skin samples, facilitated by variations in reflectivity in the THz range caused by differences in hydration levels between cancerous and healthy cells. [7]

High resolution THz rotational spectroscopy is facilitated by interactions between the terahertz radiation and quantized molecular rotational transitions of polar molecules. THz molecular spectroscopy relies on the interaction between electromagnetic radiation and the permanent electric or magnetic dipole moments in polar molecules to produce spectra. Thus, molecules without permanent dipole moments will have no spectra, or much weaker spectra rising from higher order multipole moments. THz rotational spectroscopy is sensitive to molecular structure. Therefore, even molecules with the same chemical makeup but different structure will have unique spectral "fingerprints." For example, acetic acid and glycolaldehyde share a chemical composition but have different molecular structures, resulting in very different rotational spectra.

A brief discussion of the quantum mechanical description of rotational spectroscopy provides a basis for understanding this uniqueness. To start, consider the rotational kinetic energy operator of a molecule:

$$K_R = \sum_{i=1}^{3} \frac{1}{2} I_i {\omega_i}^2 = \sum_{i=1}^{3} \frac{{J_i}^2}{2\, I_i}$$

Eq. 1.1

In the above equation, K_R represents the total rotation kinetic energy, I_i represents the moment of inertia, ω_i represents projection of the angular velocity, J_i represents the total angular momentum, and index i represents spatial coordinates. Consider the simple case of an azimuthally symmetric linear molecule where $I_x = I_y = I$ and $I_z = 0$, such as carbon monoxide (CO). Assuming that the molecule is a rigid rotor, the Hamiltonian operator in this case is:

$$\hat{H} = \frac{\hat{J}^2}{2I}$$

Eq. 1.2

and the 1-dimensional time-independent Schrodinger equation yields[1]:

$$\frac{\hat{J}^2 \psi}{2I} = E \psi$$

Eq. 1.3

$$E = \frac{J(J+1)\hbar^2}{2I}$$

Eq. 1.4

From Eq. 1.4 a function for energy, E, in terms of angular momentum quantum number J can be defined.

$$E(J) = J(J+1)B$$

Eq. 1.5

where B is a constant equal to $\hbar^2/2I$. The transition frequency difference, ν, between two adjacent energy states is:

[1] No potential energy term for sake of illustrating the simplest case (rigid rotor).

$$v = \frac{E(J+1) - E(J)}{h} = \frac{2B}{h}(J+1)$$

Eq. 1.6

This shows that for an azimuthally symmetric rigid linear molecule, the energy gap between two adjacent rotational states is inversely proportional to the moment of inertia. This is, however a simplified case. In reality, the potential term will not be zero. In addition, there may be unique moments of inertia in each coordinate direction, resulting in a 3-dimensional Schrodinger equation with 3 rotational constants (commonly referred to as *A*, *B*, and *C*) dependent on molecular structure and orientation. These coefficients grant knowledge of both the moments of inertia about the coordinate axes and the geometry of the molecule. In addition, these coefficients provide the ability to predict the rotational spectra of the molecule with spectroscopic accuracy.

1.3 Rotational Spectroscopy and Gas Chromatography Mass Spectroscopy

Terahertz rotational spectroscopy is particularly good at identifying and distinguishing many of the volatile organic compounds [VOCs] that are found in human breath. While gas chromatography-mass spectroscopy [GC-MS] is widely adopted in identifying these compounds, and considered to be a golden standard, THz rotational spectroscopy has several distinct advantages. THz rotational spectroscopy is capable of the high sensitivity necessary to identify most VOCs of interest. In addition to the sensitivity, sensors utilizing THz spectroscopy have a very low false alarm rate due to the uniqueness of molecular spectral fingerprints. The system employed in this study has demonstrated the ability to detect chemicals with concentrations into the parts per trillion [ppt] with near zero probability of false alarm. [8] In addition, THz rotational spectroscopic systems can be relatively inexpensive, especially when compared with GC-

MS. [9] THz spectroscopy can also be done much faster than GC-MS, allowing for much quicker sample analysis.

Chapter 2

2.1 Cell Lines and Media Types Used

One of the objectives of this thesis was to ascertain metabolic differences between human cell types using THz molecular spectroscopy as a tool to differentiate gaseous metabolites. Thus, several types of cells were involved in this study in order to determine whether metabolic behavior was consistent across different types of cells and to establish whether cell cultures could be identified based on metabolism of compounds of interest. The primary investigations focused on lung cells. Both immortal (cancerous) and primary (healthy) cell lines were used. The cancerous Cultured Human Airway Epithelial [Calu-3] cell line was established in 1975, originating from a 25-year-old Caucasian male with adenocarcinoma of the lung. [10] Growth medium for the Calu-3 cell cultures consisted of Roswell Park Memorial Institute medium [RPMI], 10% Fetal Bovine Serum [FBS] (dissolved in water), and 0.5% penicillin streptomycin. Discussion of use of Calu-3 cells and medium in the experiment can be found in Chapter 3. A complete list of the components of the medium used can be found in Appendix 2.

Human primary epithelial airway cells were extracted from a healthy human donor at the University of Iowa. Demographic information was not made available in accordance with the Institutional Review Board of the University of Iowa (IRB ID No. 9507432). [11] The base growth medium, hereafter called complete F-medium, consisted primarily of Dulbecco's Modified Eagle's medium [DMEM], F-12 nutrient mixture, 10% FBS, 0.5% glutamine, 0.5% penicillin streptomycin, and other growth factors. More detailed review of medium components is left to Appendix 2. Use of these cells in the

experiment is discussed in Chapter 3. Figures and results involving use of primary epithelial airway cells in this study can be found in Chapter 4.

Spectral libraries currently available allow for the quantification of ethanol and methanol, the alcohols involved in this experiment, and acetaldehyde and formaldehyde, the products of the breakdown of these alcohols. Metabolism of alcohols in the human body is thought to primarily occur in the liver, [12] thus we chose to study liver cells in addition to lung cell cultures. Liver hepatocellular carcinoma [Hep G2] cells were used. This immortal cell line was derived from liver tissue of a 15-year-old Caucasian male with well-differentiated hepatocellular carcinoma. [13] Growth medium for Hep G2 cultures is comprised of Eagle's Minimum Essential medium [EMEM], 10% FBS solution (dissolved in water), and 0.5% penicillin streptomycin. Further discussion of the components of this medium can be found in Appendix 2. Results involving Hep G2 cells and media are presented in Chapter 4. All cell types were cultured in accordance with established protocols in the Excoffon lab at Wright State University.

2.2 Bio-Relevance and Metabolic Pathways of Ethanol and Methanol

The spectroscopic system utilized in this study can detect several metabolic VOCs relevant to bio-chemistry. The target species for this study were ethanol, acetaldehyde, methanol, formaldehyde, and acetone. Spectral libraries for each of these compounds were developed prior to this investigation. [2] A brief summary of the bio-relevance of these volatile organic compounds follows.

Ethanol, also referred to as ethyl alcohol, is primarily consumed by adults in alcoholic beverages. Ethanol is commonly found in ripe fruit and is often consumed as part of a normal diet even in those who do not drink alcoholic beverages. Endogenous

ethanol exists in the human body as a result of fermentation. [14] Ethanol generally has no adverse effects at natural biological levels. However, ethanol in significant quantities leads to intoxication and in extreme cases, death. Chronic consumption has serious biological effects, including cancer, addiction, harm to vital organs, and alteration of metabolism.

Methanol, sometimes referred to as methyl alcohol, is the simplest alcohol. Like ethanol, methanol naturally exists in the human body in minute quantities. However, methanol is harmful in much smaller quantities than ethanol. Methanol is highly toxic, and consumption can lead to permanent blindness, coma, and death. Methanol itself can depress the central nervous system, with potentially fatal results. The metabolites of methanol, formaldehyde and formic acid, also have harmful effects. [15]

In the human body, the primary pathway for metabolism of alcohols follows a relatively simple pathway, depicted in Figure 2.1. Alcohol is oxidized by an alcohol dehydrogenase [ADH] enzyme, resulting in an aldehyde. Then, an aldehyde dehydrogenase [ALDH] enzyme oxidizes the aldehyde to make a carboxylic acid, which is further metabolized and excreted from the body.

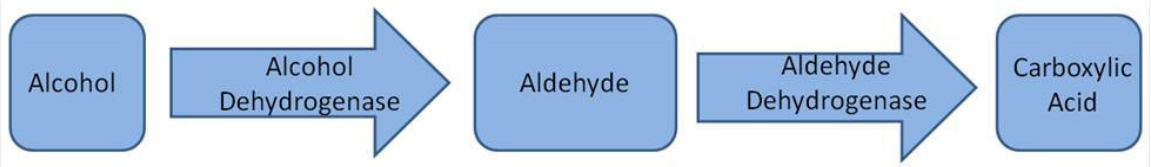

Figure 2.1: Primary metabolic pathway of alcohol in the human body.

Several different forms of alcohol dehydrogenase are present in the human body. These enzymes are divided according to class. Each class is encoded by different genes with members of the same class representing isozymes. [16] Table 2.1 displays the

different types of alcohol dehydrogenase, as well as the role of each in the body, and which organs it is active in. Class I alcohol dehydrogenase [ADH1] is primarily responsible for the metabolism of ethanol and has several subtypes: ADH1A, ADH1B, and ADH1C. Though most alcohol is metabolized in the liver, ADH1B has been found in lung tissue. [12] ADH5 is a class III enzyme that exhibits little activity for ethanol oxidation. It does, however, take on the role of breaking down formaldehyde, and is also categorized as a glutathione-dependent aldehyde dehydrogenase. In a study that compared expression of the genes that regulate ADH in the liver between healthy liver cells and Hep G2 cells, ADH1A, ADH1B, ADH1C, and ADH7 were not detected in Hep G2 cells. However, ADH4, ADH5, and ADH6 were upregulated in Hep G2 cells compared with healthy hepatocytes. [17] Thus, it is expected that cancerous liver cells will have much lower rates of ethanol metabolism compared with healthy liver tissues. The specific form of alcohol dehydrogenase responsible for the breakdown of methanol into formaldehyde is known as methanol dehydrogenase. The pathway from alcohol to aldehyde is not always one-way. While the typical operation is to oxidize alcohol to enzyme, alcohol dehydrogenase is also capable of reducing an aldehyde to an alcohol. [18]

Enzyme	Class	Function	Tissues	Additional Notes
ADH1A	I	Ethanol Metabolism	Liver	
ADH1B	I	Ethanol Metabolism	Liver, Lung	
ADH1C	I	Ethanol Metabolism	Liver, Stomach	
ADH4	II	Retinol Metabolism	Liver, Cornea	Optimized for long-chain alcohols
ADH5	III	Formaldehyde Metabolism	Most Tissues	Virtually no activity for ethanol oxidation
ADH6	IV		Liver, Stomach	
ADH7	V	Retinol Dehydrogenase	Liver, Stomach	Inefficient ethanol oxidation

Table 2.1: Forms of alcohol dehydrogenase, including function and the tissues in which they are found. [12]

Acetaldehyde is the result of alcohol dehydrogenase acting on ethanol. Acetaldehyde is a known carcinogen in sufficient quantities. Acetaldehyde is an oxidizing agent and can destroy cell walls in sufficiently high concentrations. In addition, acetaldehyde can bind to proteins, inhibiting the effectiveness of these proteins. [19]

Formaldehyde has toxic effects on the central nervous system and is a known carcinogen in sufficient quantities. [20] Excess formaldehyde has been shown to increase glucose consumption. [21] Formaldehyde is also an oxidizing agent, enabling the breakdown of lipid-based cell membranes. [22]

Due to the potential for harmful effects of aldehydes on the body, there are multiple pathways for elimination of these compounds. Aldehydes are broken down into carboxylic acids by the aldehyde dehydrogenase [ALDH] enzyme. Table 2.2 contains selected forms of ALDH and their functions. The forms of ALDH that are responsible for oxidizing acetaldehyde to acetic acid are ALDH1A1, ALDH1B1, ALDH2, and ALDH5. [12].

Formaldehyde is metabolized to formic acid by ALDH. Formaldehyde is primarily metabolized by glutathione-dependent formaldehyde dehydrogenase (AHD5), though other non-specific ALDHs act on formaldehyde as well. [20] ADH1 also acts on formaldehyde and has been observed both oxidizing formaldehyde to produce formic acid, and reducing formaldehyde to produce methanol. [23] In the aforementioned study comparing Hep G2 cells to healthy liver cells, ALDH1A1, ALDH1B1, and ALDH2 were downregulated in Hep G2 cells compared with healthy liver cells. ALDH5A1 was upregulated compared with healthy hepatocytes. [17]

Another pathway by which the body metabolizes aldehydes involves neutralization by antioxidants. Antioxidants can be either enzymatic or non-enzymatic and reduce potentially harmful reactive oxygen species. [24] In particular, glutathione is a non-enzymatic antioxidant found in most body tissues that prevents reactive oxygen species (such as acetaldehyde and formaldehyde) from damaging important cellular components. [24]

Enzyme	Tissue	Function
ALDH1A1	Liver	Acetaldehyde Metabolism
ALDH1B1	Liver	Acetaldehyde Metabolism
ALDH2	Liver	Acetaldehyde Metabolism
ALDH5A1	Liver	Acetaldehyde Metabolism

Table 2.2: Forms of aldehyde dehydrogenase relevant to study in acetaldehyde and formaldehyde.

Carboxylic acids are eliminated through several pathways. Acetic acid is further metabolized to acetyl-CoA which is then reduced to water and carbon dioxide through the citric acid cycle. [25] Formic acid is further metabolized to produce carbon dioxide and water, but is also excreted unchanged in small quantities. [26]

2.3 Glucose Metabolism

The primary source of energy for cells in mammals is glucose. Insulin is used by the body to regulate cellular glucose intake and use. When insulin levels drop, glucose transport slows or stops and cells are required to find alternate sources of energy. [27] This is effectively what occurs in Type I Diabetics. As cells begin to run short on glucose, they begin to metabolize fatty acids into ketones as a source of energy. [27] One such ketone produced in this low-glucose environment is acetone. The spectroscopic system used in this thesis is sensitive to acetone in trace quantities. As discussed before, the medium used with primary lung cells comes in high and low glucose varieties and has

insulin added, lending itself to testing low glucose and no-insulin scenarios. Based on prior research, it is anticipated that as glucose and insulin are depleted, acetone will be produced. [27]

Chapter 3

3.1 Collection of Cellular Gaseous Metabolites

The aim of the experiment was to evaluate the gaseous metabolic expression of cell cultures, to gauge the capabilities of THz chemical sensing in this application, and to validate the hypothesis that cell cultures can be differentiated based on their gaseous metabolites. A metabolic gas collection system was designed to aid in this endeavor. Figure 3.1 is a graphical representation of the collection setup used in this experiment.

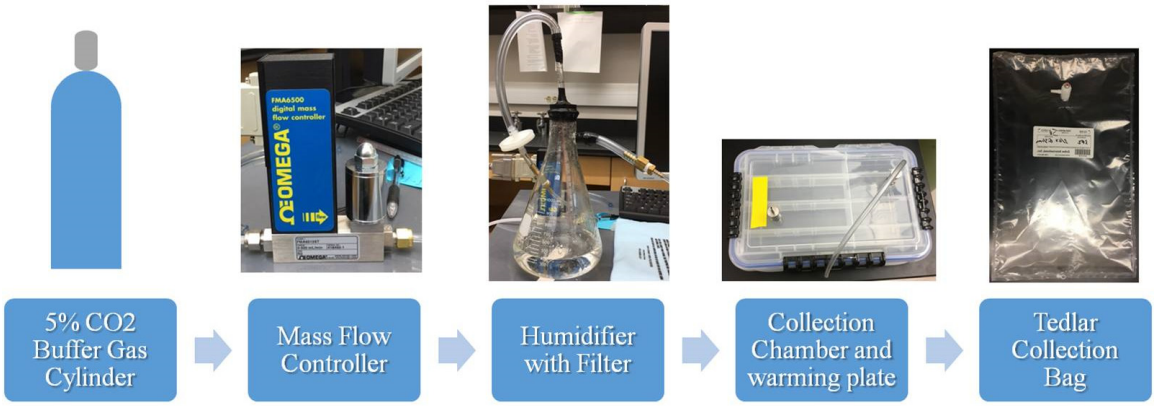

Figure 3.1: Schematic of the collection system used in the experiment.

Gas flow from a tank containing 5% CO_2 in dry air to the system was regulated by an Omega FMA6500 digital mass flow controller. The mass flow controller regulated the gas flow rate at 15 standard cubic centimeters per minute. The gas passed through a custom-built humidifier (a tube submerged in distilled water), introduced to provide moisture to the cell cultures. Figure 3.2 depicts the humidifier used in the experiment. The gas mixture then entered into the enclosure containing cell cultures. Figure 3.3 shows the cell culture enclosure. The enclosure consists of an airtight box with two ports, one on either end of the box. A 24-well plate containing cell cultures was placed inside the airtight enclosure with humidified air - CO_2 gas mixture flowing above the surface of

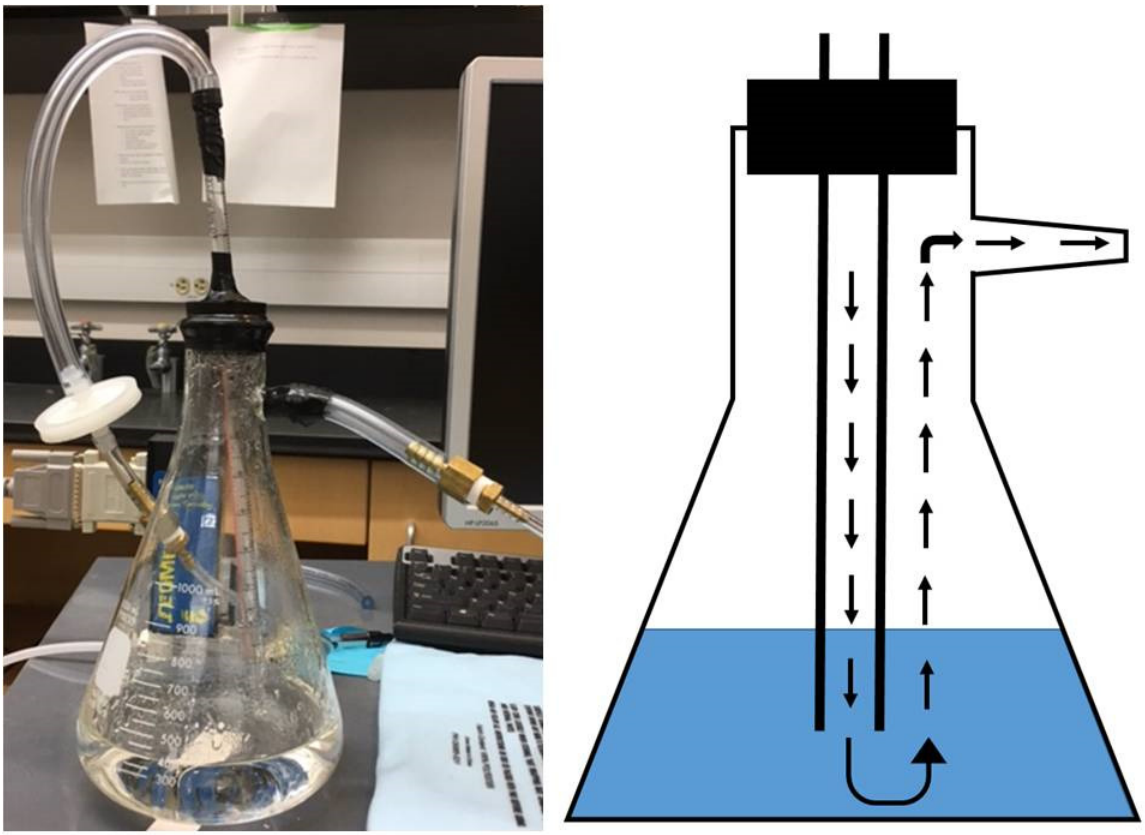

Figure 3.2: Photograph and diagram of the humidifier used for providing moisture to the cells. Gas enters the humidifier through a hollow tube inserted through the rubber stopper, bubbles up through the water, and leaves through an open valve in the side of the flask.

each well containing cells submerged in growth medium. Figure 3.4 contains diagrams depicting two possible configurations for cell culture in nutritional media. For the samples discussed in this thesis, cells were cultured submerged in medium as in Figure 3.4(b). Future experiments will involve cells at the air-liquid interface as depicted in Figure 3.4(a). Gas entered the enclosure through one of the ports, flowed over the 24-well plate, and exited through the other port, flowing into a Tedlar bag. A warming plate was used to maintain the temperature of the enclosure at 37º C to simulate in vivo conditions. Collections were made over a span of 2.5 hours, corresponding to a total volume of 2.25 liters. All collections were made under these conditions to preserve consistency.

Figure 3.3: Photographs of the cell enclosure. Pictured left is the enclosure showing the ports with tubing attached to one of the ports. Pictured right is the enclosure including a 24-well plate with medium.

A baseline of gaseous composition was established for each cell line by collecting samples from the respective media and their sub-components. These baselines served as a point of comparison for the cell culture samples. By comparing dilutions for each VOC of interest, the difference between samples with and without cells can be calculated. Refer to Appendix 2 for a discussion of the components of each medium. Results of the media-only collections can be seen in Chapter 4.

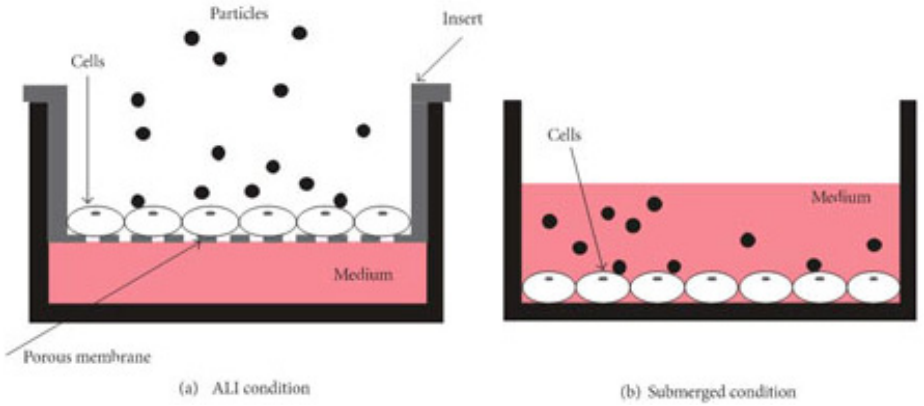

Figure 3.4: Schematics of two cell media configurations. (a) Cells cultured on a permeable membrane and placed at the air-liquid interface. (b) Cells cultured on the bottom of a well and submerged in medium. [28]

In each of the cell lines, comparisons were made between plain medium (referred to hereafter as control medium), ethanol-doped medium, methanol-doped medium, and acetaldehyde-doped medium. Each series of data collections consisted of pairs of corresponding collections including a medium-only collection and a collection of medium plus cell culture. For example, a single series would consist of : 1. control medium and control medium and cells; 2. ethanol-doped medium and ethanol-doped medium and cells; 3. methanol-doped medium and methanol-doped medium and cells; and 4. acetaldehyde-doped medium and acetaldehyde-doped medium and cells. For each pair of collections, media came from the same batch. Samples were doped in order to probe metabolic responses to increased levels of ethanol, methanol, and acetaldehyde, in an attempt to differentiate cell cultures based on their metabolic response rates. Because such small concentrations of each chemical were added, adding chemical to each well of the 24-well plate would have been inconsistent between each well. Instead, a known quantity of each chemical was diluted in distilled water. This water mixture was then added to the medium in known quantities to obtain the desired dilutions. In the case of doped media, cells were grown and maintained in a standard medium environment until immediately before collection, at which point the medium was changed to the doped state.

Following each collection, cells were returned to the incubator in which they were grown. Images were taken immediately following collections and again after 48 hours to ensure cells were surviving. Figure 3.5 includes two such images for a selected set of Calu-3 cells. As can be seen in the figure, cell morphology remained intact, indicating cell survival. Cells did not mutate or change shape as a result of the experiment. No

contamination of the cells is visible. No organisms other than the cells is visible in the photographs, indicating that cells were not contaminated while in the enclosure. There is a marked increase in cell density in the second image, indicating that cells continued to grow after the sample collection was complete. Images were taken at 10x magnification with a Nikon Eclipse TE2000-S microscope. Contrast was increased to better show cell outlines. Collectively, the images taken confirmed survival of cells during the 2.5 hour collection period.

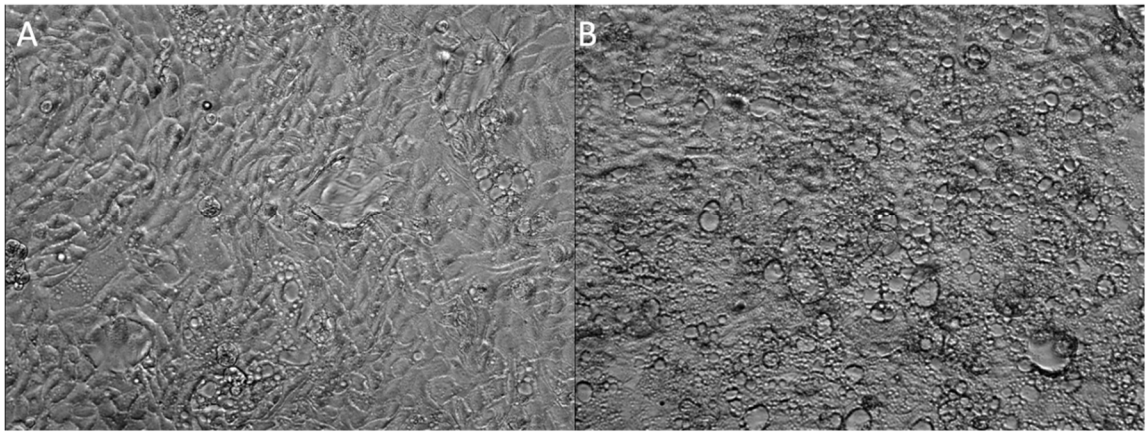

Figure 3.5: (A) Photograph of Calu-3 cells taken immediately after a run in which medium was doped with 10 ppm methanol. (B) Photograph of Calu-3 cells taken 48 hours after the run.

3.2 THz Spectroscopic Technique

The spectroscopic system used for this study was based on prior research, [2] and consisted of a THz transmitter and receiver, utilizing solid state harmonic multipliers, driven by a pair of microwave synthesizers purchased from Virginia Diodes. A schematic of the spectroscopic system used can be found in Appendix 1. A 10 MHz rubidium clock provides the frequency used to drive these synthesizers. Signals from the microwave synthesizers operating in 11.6 to 15 GHz range were harmonically multiplied by a factor of 18 by the THz transmitter and receiver. THz radiation was collimated along the axis of

a 2-meter long absorption cell with a volume of 14 liters. Lenses made of high density polyethylene were use for collimation of source radiation and to focus the radiation transmitted through the cell into the detector on the other end of the vacuum chamber. Lenses were slightly rotated to reduce standing wave effects. The system was operated in the 210 to 270 GHz region to utilize previously developed spectral libraries. For each VOC, several strong spectral lines were chosen for detection. Selecting multiple lines allows for more accurate detection and provides a means of dealing with potential spectral overlaps between various chemicals. To probe these lines, the system swept 2.5 MHz in either direction from line center to create 5 MHz snippets. Data scans were governed by predetermined lists of snippets containing strong lines of the chemicals of interest. Defining snippets reduced the time required for data acquisition by probing regions only where lines were known to exist. The master synthesizer, controlling the signal going to the transmitter, stepped through the line center frequencies. Table A.9 in Appendix 3 contains the center frequencies of each snippet for the compounds relevant to this study. The THz source was FM modulated by the microwave synthesizer at a rate of 31 kHz and a depth of modulation [DOM] of 400 kHz. The slave microwave synthesizer provided signal to the heterodyne receiver and tracked the master synthesizer at an offset of 93 MHz. The signal from the slave synthesizer is multiplied by the receiver by a factor of 18 and the resulting frequency is mixed with the signal from the transmitter. The resultant of this mixing signal at the intermediate frequency of 1.674 GHz was converted to a DC (direct current)-coupled signal proportional to its amplitude by a Herotek DHMA18Ab zero-bias Schottky diode detector. [9] Output of the diode detector was amplified by a Stanford Research Systems [SRS] SR560 low-noise amplifier before

going to a Zurich Instruments HF2LI lock-in amplifier which simultaneously provided first derivative and second derivative signal outputs.

The spectrometer and data collection were controlled by a computer. Each data collection began with a power baseline scan. Figure 3.6 displays a typical DC-coupled power spectrum. These scans involved turning off FM modulation and directly acquiring

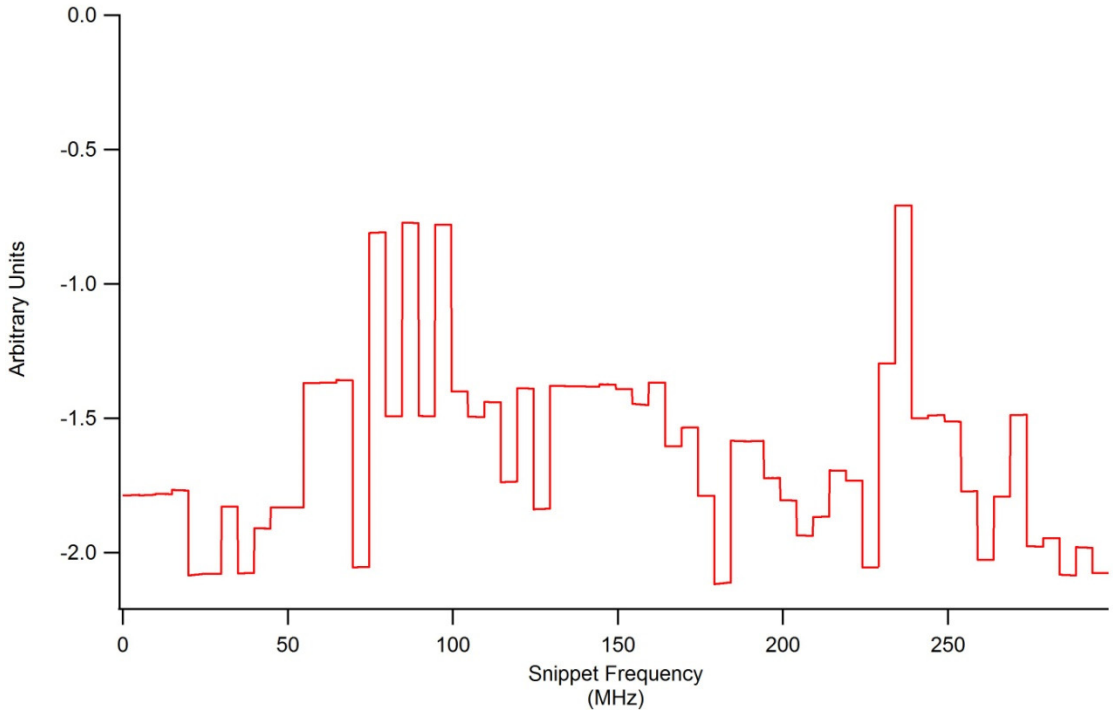

Figure 3.6: Sample DC power spectrum.

the DC-coupled output of the SRS SR560 amplifier. DC-coupled baselines were used to determine transmission power at each snippet frequency and were used to normalize the spectral intensities by the system's power. To maximize the dynamic range of the data acquisition system, spectra were then collected with the SRS amplifier in AC-coupled mode and with frequency modulation enabled. To identify any residual contaminants remaining in the absorption cell of the spectrometer from previous samples, spectra of an empty cell closed off from vacuum pump were collected. These chemical history scans

were conducted with the SRS SR560 low noise amplifier in AC-coupled mode. Figure 3.7 shows the spectrum of one such chemical history scan. Data from four channels was collected from the Zurich instruments lock-in amplifier. Two of these channels were the first derivative signal collected 90 degrees out of phase with respect to one another. The other two channels were the second derivative signal, also 90 degrees out of phase.

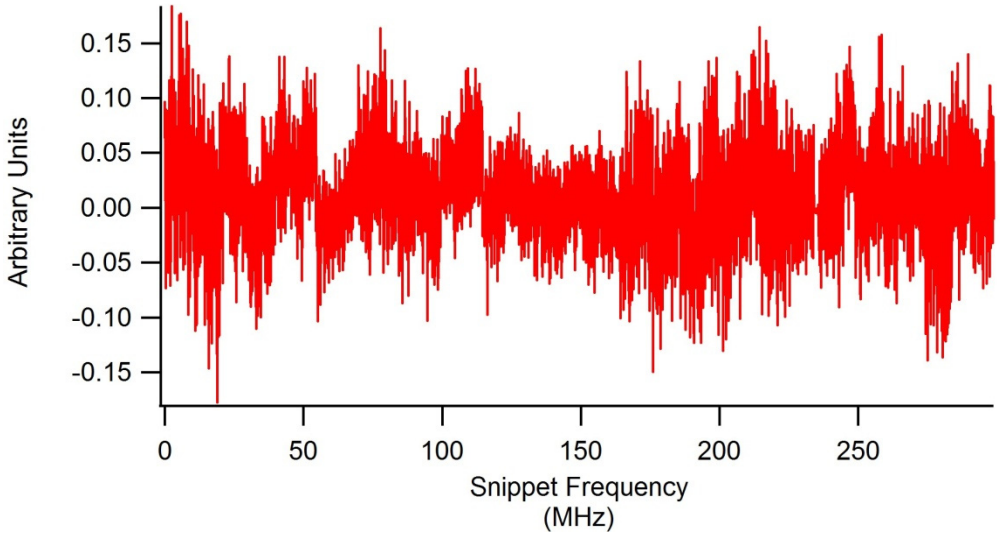

Figure 3.7: Spectrum of a typical chemical history scan.

Once the DC-coupled baseline and chemical history had been established, the sample was preconcentrated. Preconcentration was conducted with an Entech 7100A preconcentrator. Preconcentration efficiencies were not involved in most calculations in this thesis, but have been measured by prior work for several chemicals. [9] Table 3.1 contains a list of chemicals and their preconcentration efficiency. Prior to preconcentration, each Tedlar bag containing gaseous samples was placed under a heat

Chemical	Preconcentration Efficiency
Acetone	52%
Ethanol	54%
Acetaldehyde	63.4%

Table 3.1: Preconcentration efficiencies for acetone, ethanol, and acetaldehyde. [9]

lamp for approximately 10 minutes to promote the detachment of molecules from the surface of the bag. Typical pressures in the absorption chamber of the spectrometer after preconcentration ranged between 9-12 mtorr. With the sample in the chamber, a snippet scan was performed. These scans were also conducted with the SRS SR560 in AC-coupled mode with a band-pass filter covering 3 kHz to 300 kHz. Eight complete passes through the snippet list were made, with each pass being saved independently to improve signal to noise ratio by averaging.

Analysis of spectral data was conducted similar to previous research. [27] Data analysis was conducted in IGOR Pro software package. [29] The eight separate passes from the snippet scan were imported and averaged to produce the final spectrum. Figure 3.8 displays the spectrum of a snippet scan, averaged over the eight passes as discussed,

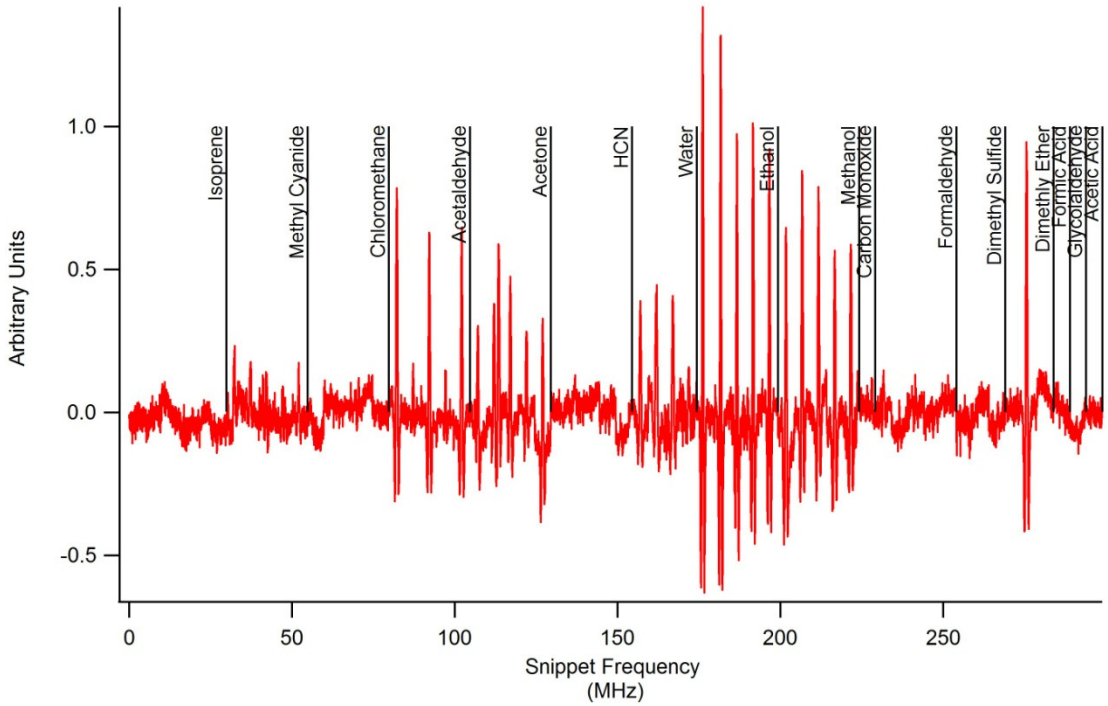

Figure 3.8: Spectrum of a snippet scan of an ethanol-doped medium sample, averaged over 8 passes.

with labels added to demarcate the snippets belonging to each chemical. The spectrum was then scaled by the corresponding DC-coupled baseline spectrum. This scaled spectrum was fitted against libraries for each chemical of interest. Figure 3.9 is an example of one of these fits. Libraries were obtained previously using pure samples at known pressures.

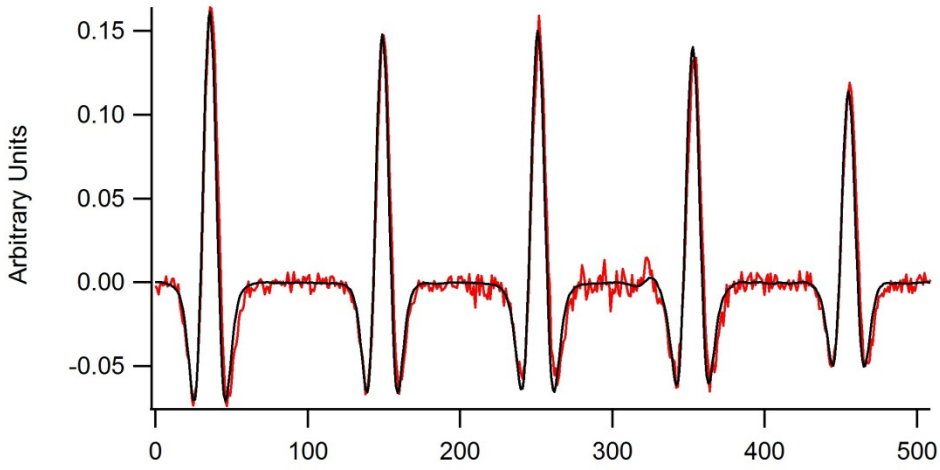

Figure 3.9: Sample plot of scaled spectrum (red) and library fit (black) for ethanol spectral lines.

Number density was calculated by comparing peak heights (done as a least squares fit) with library spectra with known number density. Partial pressures were calculated by dividing calculated number density of each chemical by the number density of ambient air. Volumetric dilution is then calculated by dividing the partial pressure by atmospheric pressure and scaled by the ratio of absorption cell volume to sample volume and sample temperature to absorption cell temperature as shown below.

$$Volumetric\ Dilution = \frac{Partial\ Pressure\ of\ Analyte * Absorption\ Cell\ Volume * Sample\ Temperature}{Atmospheric\ Pressure * Sample\ Volume * Absorption\ Cell\ Temperature}$$

Eq. 3.1

The partial pressure of the analyte was determined spectroscopically. The absorption cell volume was 14 L, the sample volume was 0.5 L, the sample temperature was room temperature (23 ^{0}C), and the absorption cell temperature was 60 ^{0}C.

Chapter 4

4.1 Results

4.1.1 Assessment of Chemical Contaminations

To properly assess metabolic expressions of cell cultures, the baseline contamination concentrations of relevant compounds were measured for a range of experimental conditions. Chemical contaminants of the overall system were identified. In order to establish these contamination baselines, several collections were made to test various environments. The cell enclosures could have chemical contamination due to prior use, thus, collections were made with empty enclosures to check for contaminants. Enclosures were placed under a heat lamp and lab air was pulled through them in an effort to clean them and remove any residual contaminants, followed by a standard sample collection sequence. Next, distilled water was placed in a 24-well plate within the enclosure and a sample collection was performed to identify any potential contaminants in the plastic ware or the water used in the experiment. The Tedlar bags used in our experiments were re-used multiple times and were purged between collections. To check for any residual contaminants, a bag was filled with high purity (Grade 5) nitrogen and a standard THz chemical analysis was performed to identify any pollutants in the system. Figure 4.1 shows the results of contamination testing. Shown in red are the spectroscopically defined sample dilutions with error bars. Error bars correspond to the uncertainties returned by the least squares fitting routine. The empty spectroscopic chamber background is shown in blue, with corresponding error bars obtained from the least squares fit. Concentration of acetaldehyde was greatest in the water sample and was on the order of 10 ppb. Acetone dilution was also highest in the water sample and was on

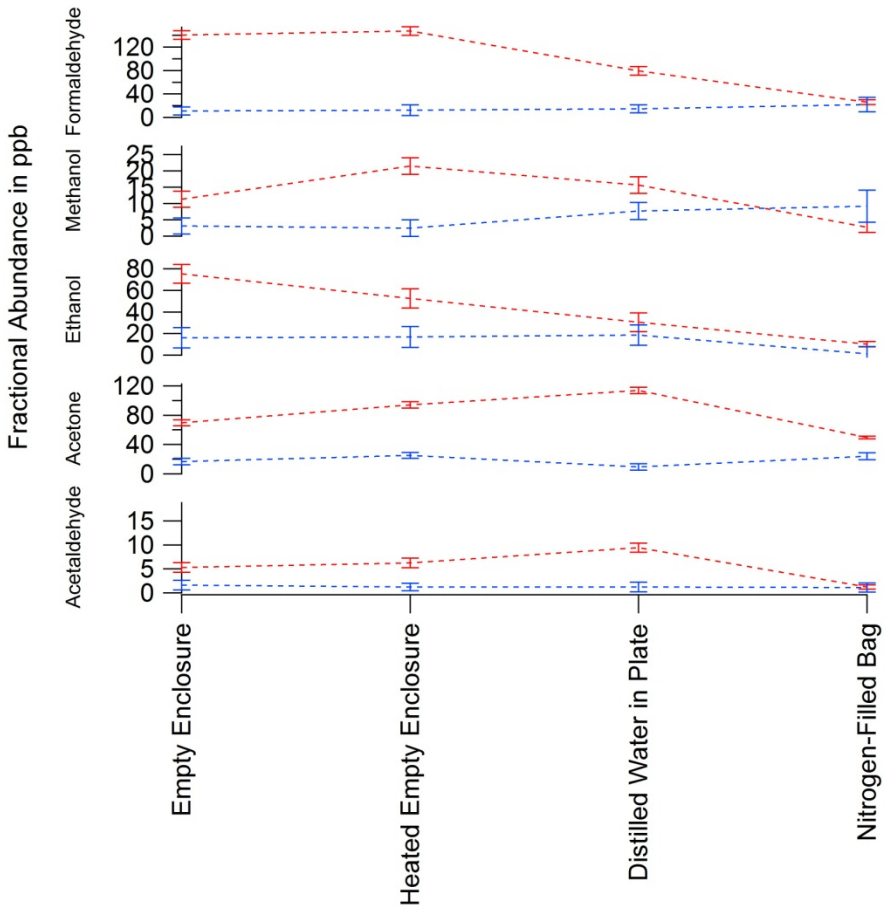

Figure 4.1: Detected dilutions in parts per billion of formaldehyde, methanol, ethanol, acetone, and acetaldehyde in samples collected in a purged empty cell enclosure, the same enclosure after being purged while heated, the same enclosure with a 24-well plate of distilled water placed inside, and a nitrogen-filled bag.

the order of 100 ppb. Ethanol contamination was greatest in the enclosure before heating and was on the order of 80 ppb. Methanol dilution was highest in the heated enclosure and was roughly 25 ppb. Formaldehyde contamination was the highest in the empty enclosure and was approximately the same in both the unheated and heated configurations. Dilution of formaldehyde was on the order of 150 ppb. In the same system, but with distilled water added, detection of formaldehyde decreased. During this and subsequent sample collections, condensation occurred on the top surface of the enclosure. It is hypothesized that this condensation cooled the enclosure, and that formaldehyde detection is a function of temperature.

4.1.2 Composition of Nutritional Media Used for Cancerous Lung Cells

To determine the baseline levels of key chemicals in the nutritional media sample, collections and analyses for each type of media were performed. Analyses of the components of media aid in understanding of what concentrations of the VOCs of interest are present in the media, and their origin. By comparing the dilutions detected in the media with those detected in cells, it can be determined whether significant changes have occurred. Figure 4.2 displays the fractional abundances in parts per billion [ppb] of compounds of interest detected in key components of Calu-3 medium. Two samples were

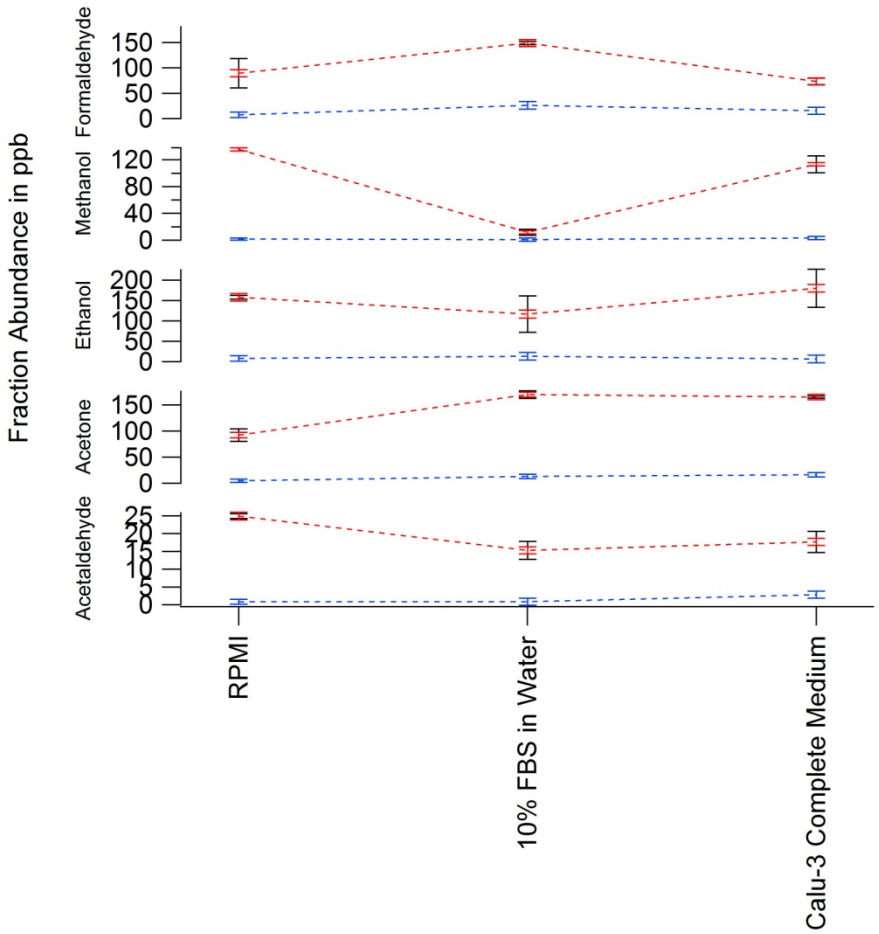

Figure 4.2: Detected dilutions in parts per billion of formaldehyde, methanol, ethanol, acetone, and acetaldehyde. Samples analyzed consisted of RPMI, 10% FBS in water, and Calu-3 complete medium, each placed in a 24-well plate inside the cell enclosure.

drawn for preconcentration and analysis from each Tedlar collection bag and processed with the spectrometer. These two data points were averaged and the appropriate error calculated. The black error bars in Figure 4.2 represent the standard deviation of the two samples that were averaged. Figure 4.2 shows in red the spectroscopically determined dilutions with error bars, and in blue the dilution values from the empty absorption cell.

For these measurements, formaldehyde levels were consistently below the contamination threshold previously determined in section 4.1.1. Methanol was significant in RPMI and Calu-3 complete medium, but was near baseline in the 10% FBS solution. The figure shows that methanol is present in the media at a concentration of approximately 120 ppb. In each component, ethanol was above baseline and exists in the media at approximately 175 ppb. Acetone levels were below contamination threshold in RPMI but rose to above threshold in the 10% FBS solution and the complete medium. Acetone dilution is approximately 150 ppb in the medium. Acetaldehyde was above baseline in each sample, and was highest in RPMI. Acetaldehyde is present at approximately 15 ppb in the medium.

4.1.3 Composition of Nutritional Media Used for Primary Epithelial Airway Cells

Figure 4.3 demonstrates the dilutions for key metabolic chemicals in components of the medium used in the experiments with primary epithelial airway cells. In the primary cell media, formaldehyde was also below the contamination threshold for all samples. Methanol was significantly above baseline in all but the F-12 medium, and was highest in the primary complete medium. Methanol concentration in the "complete medium" was approximately 75 ppb. Ethanol concentrations in the complete medium are

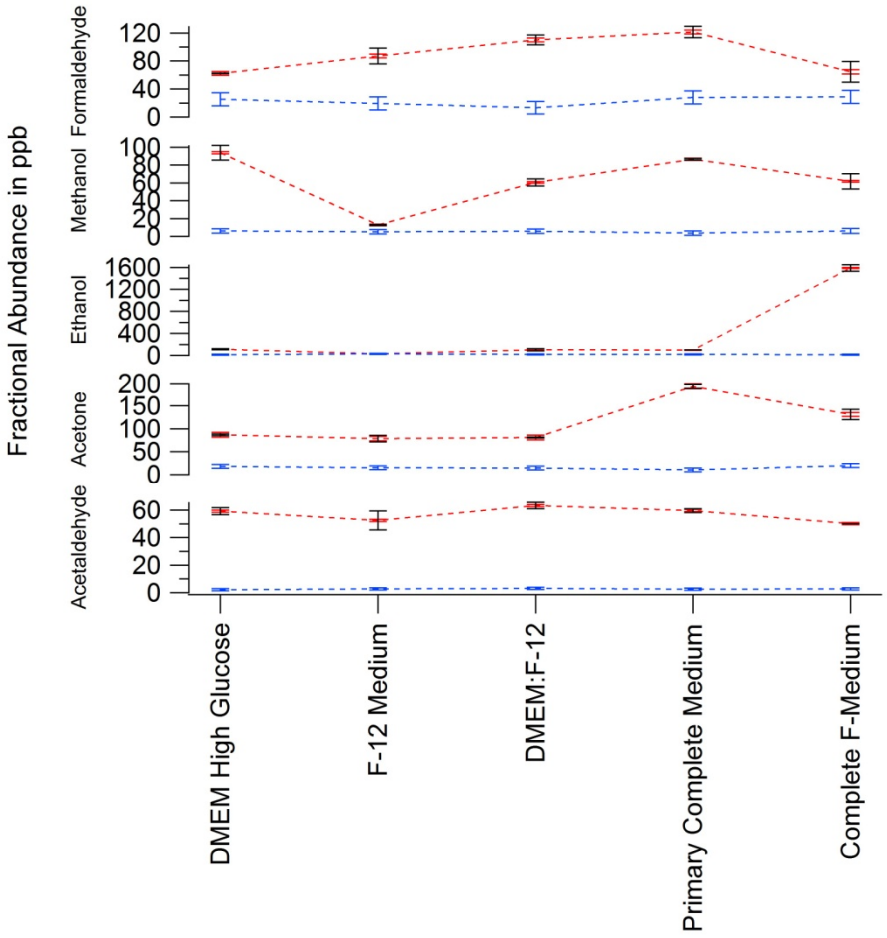

Figure 4.3: Detected dilutions in parts per billion of formaldehyde, methanol, ethanol, acetone, and acetaldehyde. Samples analyzed consisted of DMEM high glucose, F-12 nutrient mixture, DMEM:F-12, primary complete medium, and complete F-Medium, each placed in a 24-well plate inside the cell enclosure.

significantly greater than for other the constituent components. The hydrocortisone that is added to the complete medium is dissolved in ethanol and most likely accounts for this increase. Ethanol concentration in the medium is approximately 1600 ppb. Acetone is only detected above contamination threshold for the primary complete medium and the complete F-Medium used with primary cells. Concentration is highest in the primary complete medium. The acetone dilution in the medium used with cells is approximately 120 ppb. Acetaldehyde is above baseline and is relatively consistent across the samples. Acetaldehyde exists in the medium at roughly 55 ppb.

4.1.4 Composition of Nutritional Media Used for Cancerous Liver Cells

Figure 4.4 exhibits the trends in dilutions of the medium used with Hep G2 cells. Formaldehyde and methanol levels are below contamination threshold for all medium components. Ethanol is above baseline for all components. The sharp increase in ethanol in the 10% FBS solution is not consistent with what was seen in the Calu-3 sample for the same solution and may be contamination in a bag from a previous experiment. Acetone concentrations are below baseline for each component. Acetaldehyde is above

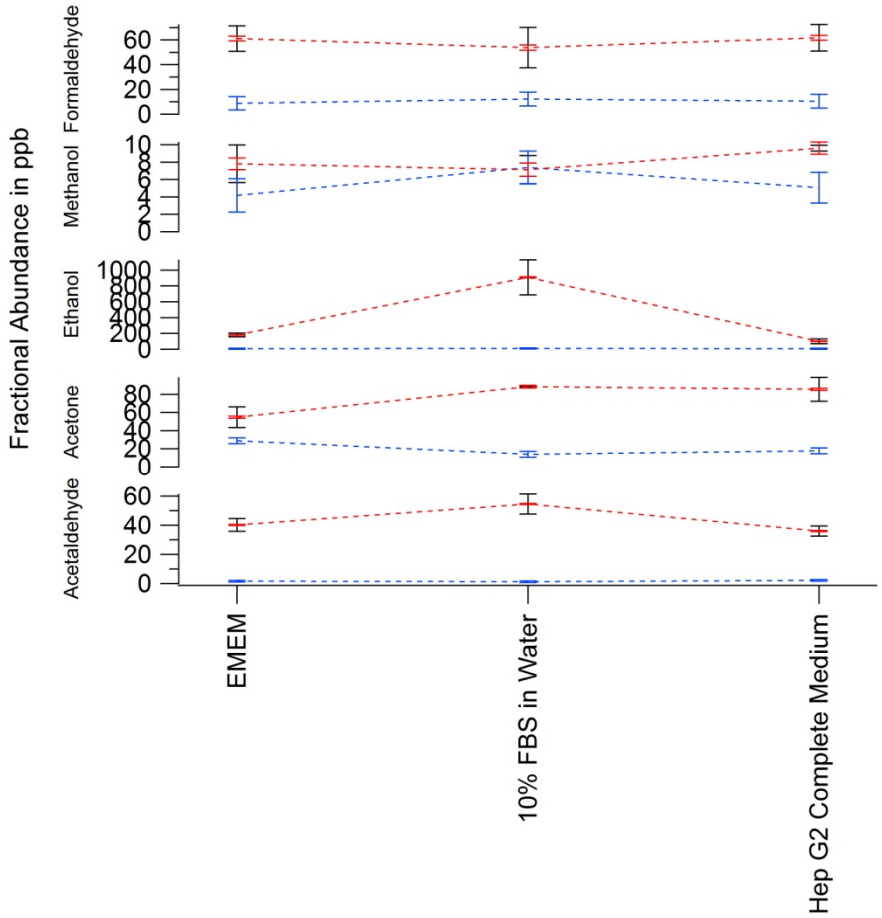

Figure 4.4: Detected dilutions in parts per billion of formaldehyde, methanol, ethanol, acetone, and acetaldehyde. Samples analyzed consisted of EMEM, 10% FBS in water, and Hep G2 complete medium, each placed in a 24-well plate inside the cell enclosure.

baseline in each component and was most abundant in the 10% FBS solution. Acetaldehyde exists in the medium at approximate dilutions of 40 ppb.

4.1.5 Cellular Metabolic Bio-Markers

With baseline concentrations of key VOCs determined, the focus was placed on evaluating metabolic rates of key VOCs. Cell media were doped immediately before sample collection with either 5 ppm or 10 ppm as discussed earlier. Figure 4.5 displays the trends in Calu-3 cells compared with media. Formaldehyde was below contamination

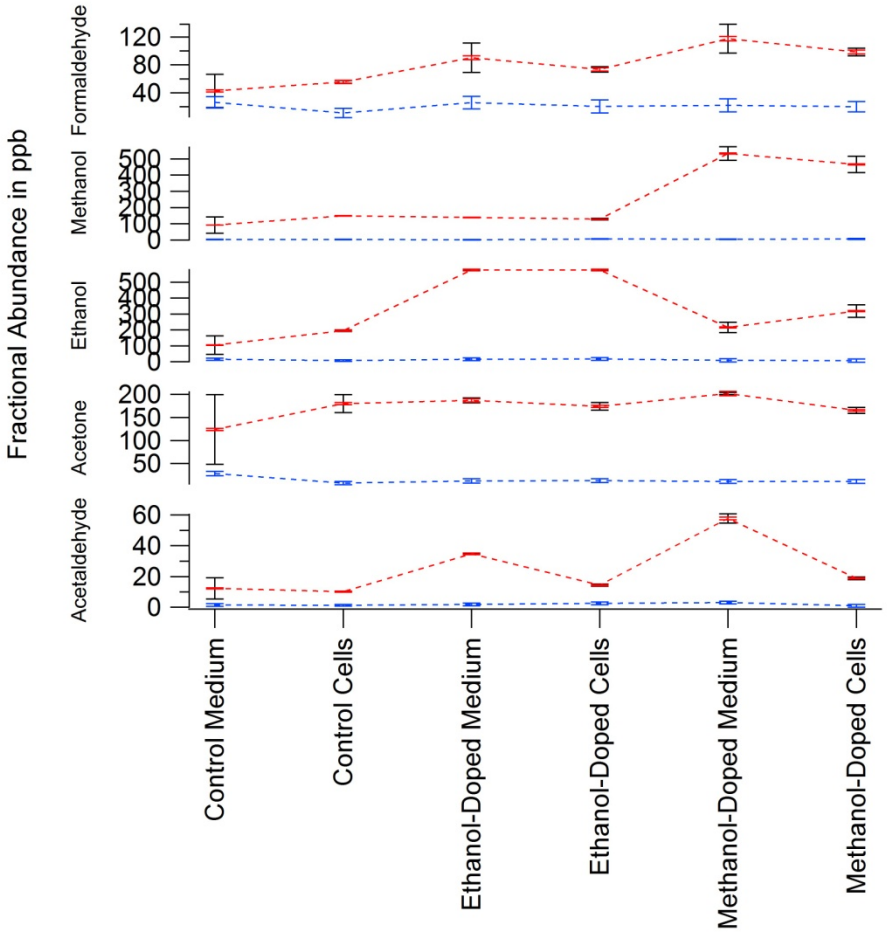

Figure 4.5: Detected dilutions in parts per billion of formaldehyde, methanol, ethanol, acetone, and acetaldehyde in the first series of Calu-3 medium and cells. Samples analyzed consisted of control medium, control cells, ethanol-doped medium, ethanol-doped cells, methanol-doped medium, and methanol-doped cells.

threshold for each sample taken. Methanol is above baseline in all samples and noticeably increases when methanol-doped media was used. When doped with 5 ppm methanol, the medium gaseous dilution-measured with THz spectrometer was approximately 500 ppb.

When cells were introduced to this medium, the measured dilution of methanol decreased to roughly 450 ppb, indicating a decrease in methanol due to the cells. Ethanol was also above the contamination limit for all collections. Doping the medium with 5 ppm ethanol resulted in an increase in ethanol detected to 500 ppb and remained at this level in the presence of cells, likely indicating the lack of enzymes necessary to convert ethanol to acetaldehyde. In addition, ethanol dilutions increased when doped with methanol in the presence of cells. Acetone was above baseline for each collection. Aside from the control medium, acetone levels were relatively constant near 175 ppb. Of particular interest is the pattern in acetaldehyde. Note the persistent decrease in acetaldehyde when cells are introduced. This pattern was observed across all cell types and for all conditions. Acetaldehyde dilutions generally increased between control group to ethanol-doped samples and again from ethanol-doped samples to methanol-doped samples. The most dramatic change in acetaldehyde was in the methanol doped samples, going from approximately 60 ppb in the medium to approximately 20 ppb. For each of the media collections, acetaldehyde dilutions were near the contamination limit.

Similar trends appear in primary airway epithelial cells as can be seen in Figure 4.6. Formaldehyde is again below the contamination threshold for all collections. Methanol is above the baseline for each sample. When doped with methanol, the dilutions for the medium and cells remained approximately the same at roughly 300 ppb. The decrease between medium and cells that was seen with Calu-3 cells was not observed

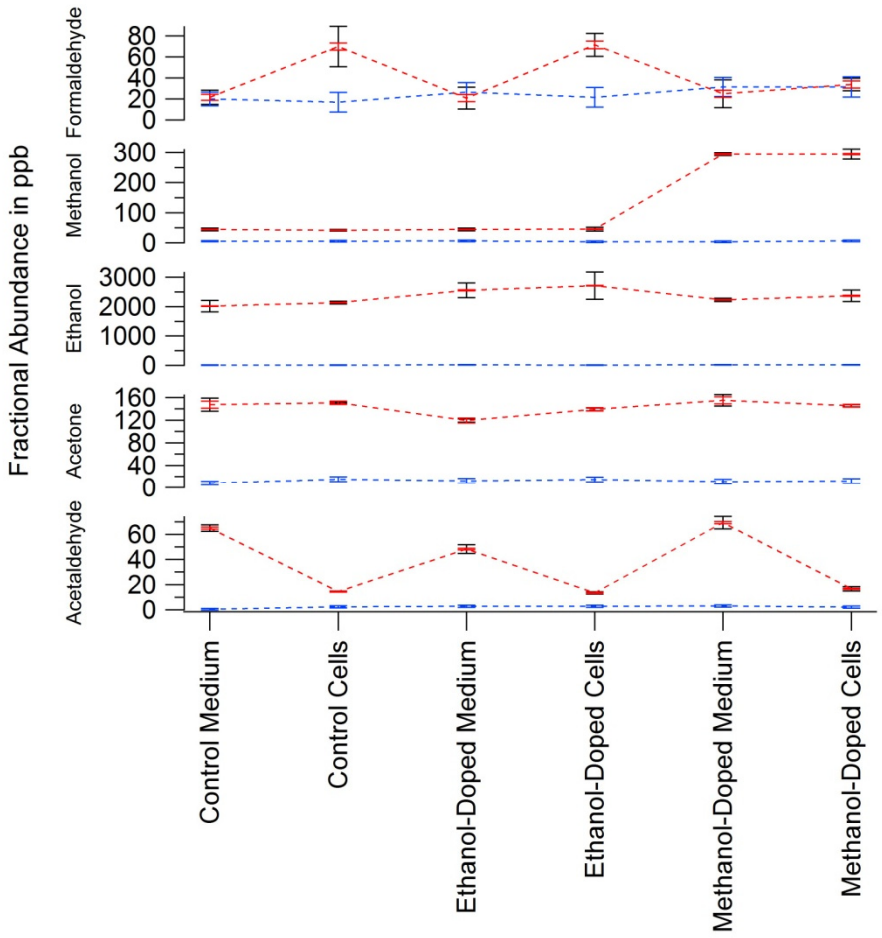

Figure 4.6: Detected dilutions in parts per billion of formaldehyde, methanol, ethanol, acetone, and acetaldehyde in the first series of primary epithelial airway medium and cells. Samples analyzed consisted of control medium, control cells, ethanol-doped medium, ethanol-doped cells, methanol-doped medium, and methanol-doped cells.

with primary epithelial airway cells. Doping with 5 ppm ethanol did not produce the desired effect of sharply increasing the measured dilutions in medium and cells in part due to the elevated levels of ethanol present in the medium. Doping with ethanol produced an approximately 500 ppb increase in both medium and cells relative to the other samples. Acetone levels were above the contamination threshold but did not significantly fluctuate between samples, remaining at approximately 140 ppb. The pattern in acetaldehyde that was first observed in Calu-3 cells was again observed with primary cells. The difference between control medium and cells is more pronounced in the

primary cells. Again, in the cell samples acetone dilutions were near the baseline. The most dramatic change between medium and cells was in the methanol-doped medium and cells. Dilutions ranged from roughly 65 ppb in the medium to 20 ppb in the cells, with values similar to the Calu-3 case.

Hep G2 cells were added later in the experiments to provide a comparison between cancerous lung and cancerous liver cells. As was noted earlier, acetaldehyde was consistently reduced to near baseline level by cells after the first series of collections from Calu-3 and primary airway cells. In order to test if acetaldehyde could be significantly increased, a fourth set of collections was added to each series to include acetaldehyde doping. Because the Hep G2 cells were added later in the experiment timeline, acetaldehyde doping was included in the first series of Hep G2 collections. Figure 4.7 shows the results of doping Hep G2 media and cells. As was the case with the other two types of cells, formaldehyde levels were below the contamination threshold. When not doped with methanol, methanol levels were below baseline. Similar to the primary cells, when doped with methanol there was a sharp increase in detected dilution of methanol in both medium and cells that was approximately the same. Methanol dilutions were approximately 600 ppb in these cases. Ethanol similarly increased to roughly 600 ppb in the doped collections. For the methanol and acetaldehyde doping, ethanol mirrors the behavior previously observed in acetaldehyde of increasing in dilution in the medium and then decreasing in the corresponding cell measurement. The range of change in ethanol dilution is much smaller than in acetaldehyde. In the collections with Hep G2 medium and cells, acetone was below the contamination threshold. Acetaldehyde levels maintain the observed trend of increased dilution in

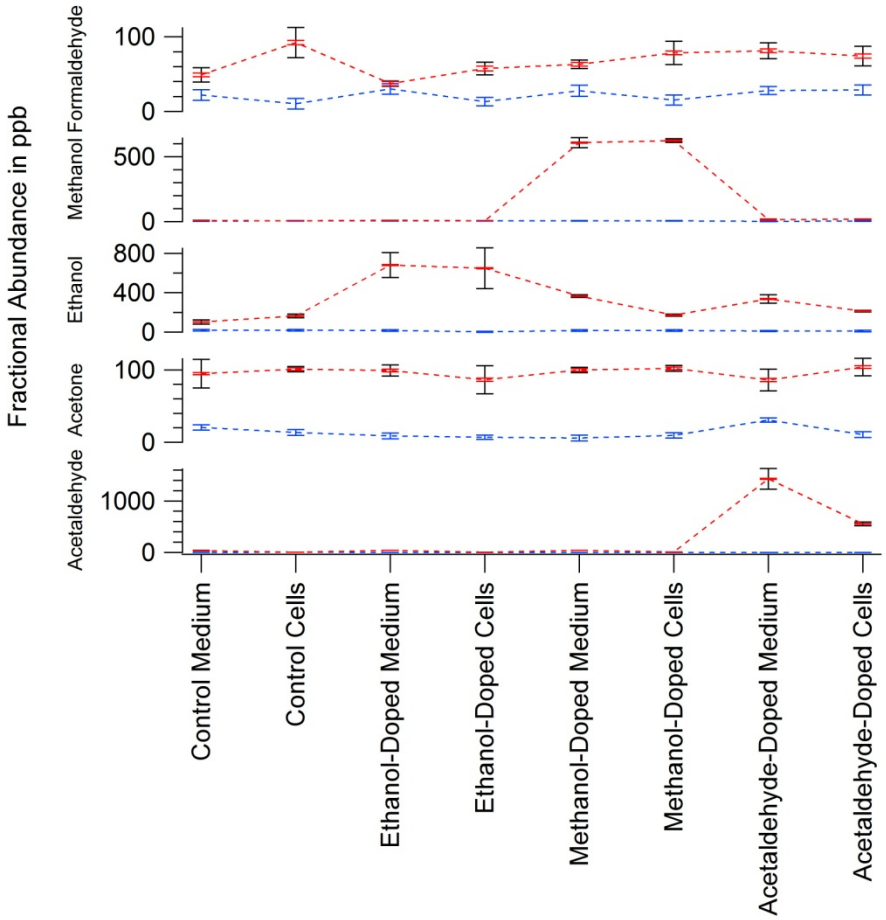

(A)

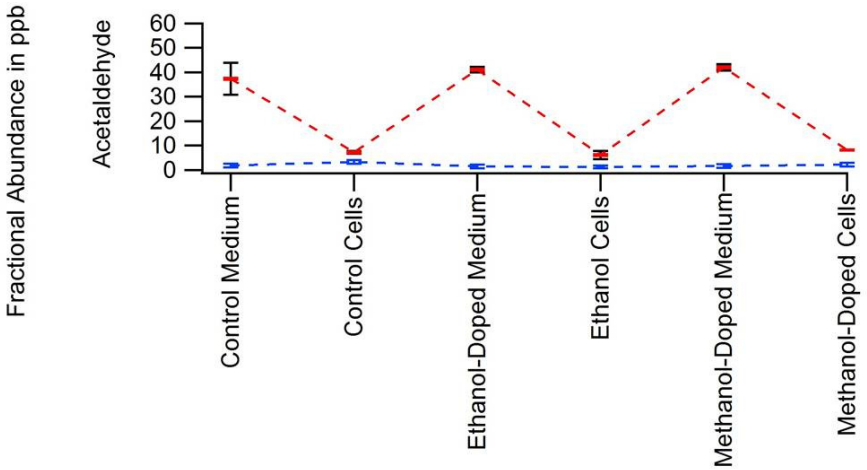

(B)

Figure 4.7: (A) Detected dilutions in parts per billion of formaldehyde, methanol, ethanol, acetone, and acetaldehyde in the first series of primary epithelial airway medium and cells. Samples analyzed consisted of control medium, control cells, ethanol-doped medium, ethanol-doped cells, methanol-doped medium, methanol-doped cells, acetaldehyde-doped medium, and acetaldehyde-doped cells. (B) Detected dilutions in parts per billion of acetaldehyde in the first series of Hep G2 medium and cells for the control medium, control cells, ethanol-doped medium, ethanol-doped cells, methanol-doped medium, and methanol-doped cells.

medium compared with the corresponding cell collection. As before, acetaldehyde levels are above baseline in medium and near baseline in corresponding cells. When doped with acetaldehyde, cells did not return the dilution to the baseline. In doped medium, dilution of acetaldehyde was measured to be approximately 1400 ppb, whereas in doped medium and cells dilution was measured to be approximately 600 ppb, resulting in a difference of 800 ppb.

In examining the data presented in the previous plots, a question arose as to the increased amount of acetaldehyde in medium as opposed to cell cultures. The enzymes that break ethanol into acetaldehyde are reversible. In order to test whether the enzymes were the source of the acetaldehyde, comparisons were made between standard media and media that was boiled to denature the enzyme proteins. Figure 4.8 demonstrates the dilution for the standard and boiled media. Formaldehyde levels were below the contamination threshold. Methanol was above the baseline in all collections, and was consistently near 150 ppb, except when the media was boiled and ethanol was added, in which case it increased to nearly 175 ppb. Ethanol was approximately 200 ppb in the medium that was not doped. Ethanol increased to approximately 800 ppb in the doped medium and nearly 1200 ppb in the medium that was boiled and then doped. Acetone was above the contamination limit for each sample, and was relatively consistent across the samples staying around roughly 150 ppb. Acetaldehyde was also above baseline for each sample. Boiling actually increased the levels of acetaldehyde. In the case where media was not doped, acetaldehyde increased by approximately 20 ppb when boiled. In the case of ethanol doping, acetaldehyde increased by approximately 40 ppb when boiled. If enzymes in the media were the source of excess methanol, ethanol, or acetaldehyde in

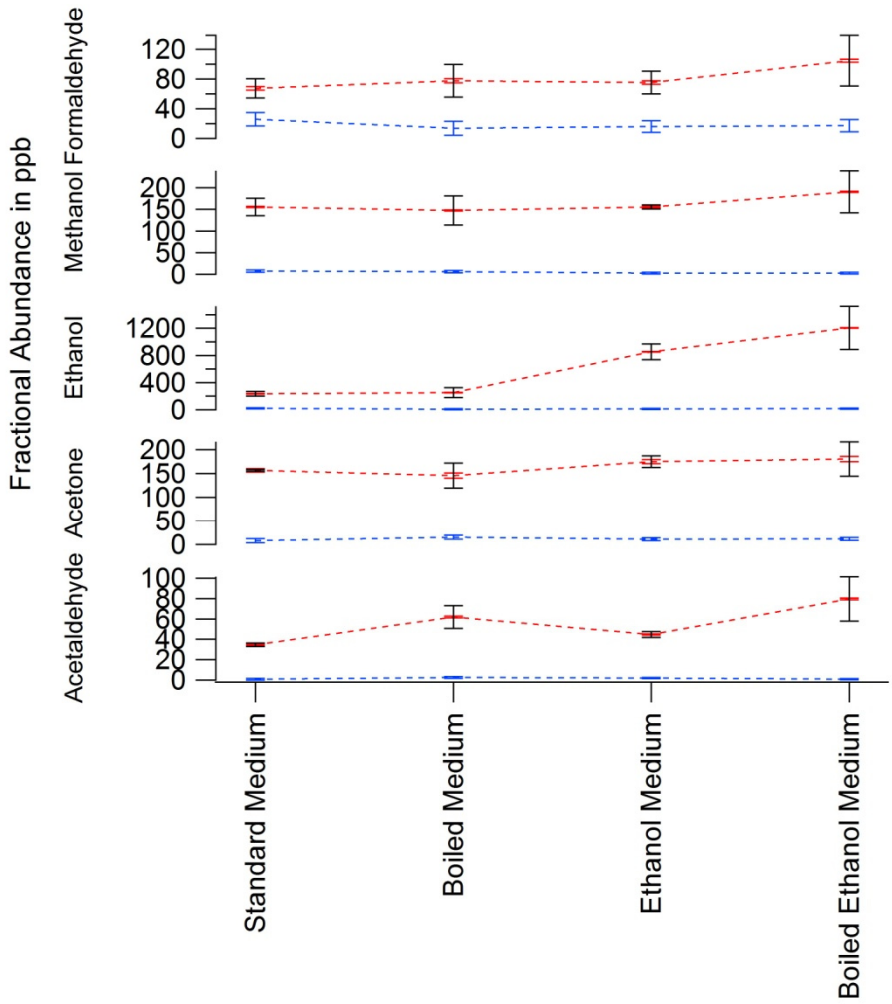

Figure 4.8: Detected dilutions in parts per billion of formaldehyde, methanol, ethanol, acetone, and acetaldehyde. Samples analyzed were a control medium, boiled control medium, ethanol-doped medium, and boiled ethanol-doped medium.

the media, then the boiled media would exhibit a decrease in acetaldehyde compared with standard media. In practice, the opposite proved true, upholding the hypothesis that it is indeed the cells that produce the change in acetaldehyde levels.

4.1.6 Detailed Investigation of Metabolic Profiles Associated with Acetaldehyde Doping

In the first series of data collection, the trend of reduction of acetaldehyde in the presence of cells was observed. It was uncertain whether the cells reduced the acetaldehyde to an effective baseline or an offset due to chemical contamination, which

would indicate complete consumption of acetaldehyde. To evaluate the behavior of cells, the first series of experiments was repeated with the addition of acetaldehyde doping. Doping was also increased to 10 ppm in an effort to produce a more prominent effect in ethanol and methanol. Figure 4.9 presents the data for the second series in Calu-3 cells. Once again, formaldehyde levels fall below the contamination threshold. Methanol was relatively consistent in the non-doped samples, hovering around 150 ppb. In the doped cases, methanol was consistently near 800 ppb with virtually no change between medium and cells. Ethanol levels behaved similarly. In the non-doped cases ethanol was near 300 ppb, with the exception of an increase to approximately 600 ppb when doped with acetaldehyde. Like methanol, there was virtually no change between medium and cells in the case of doping, both having dilutions of approximately 1000 ppb. Acetone was above the baseline in all of the collections, but did not deviate significantly from the average, near 175 ppb. The pattern of depletion of acetaldehyde by cells was observed. Of interest is the fact that acetaldehyde was not reduced to the average baseline by the cells when doped with either methanol or acetaldehyde. As before, acetaldehyde increased in the medium when doped with methanol, suggesting possible presence of acetaldehyde in the methanol sample. For each non-acetaldehyde doped case, the change between medium and cells was approximately 40 ppb. The change in acetaldehyde dilution between medium and cells when doped with acetaldehyde was from approximately 2200 ppb to 1500 ppb, a 700 ppb reduction.

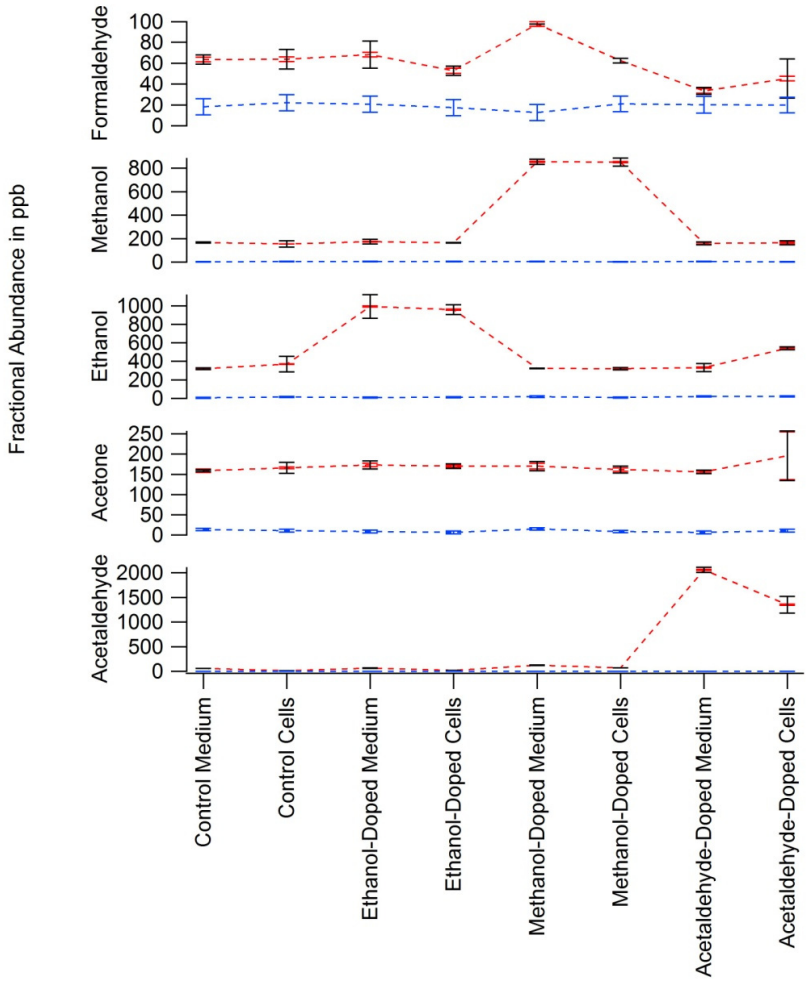

(A)

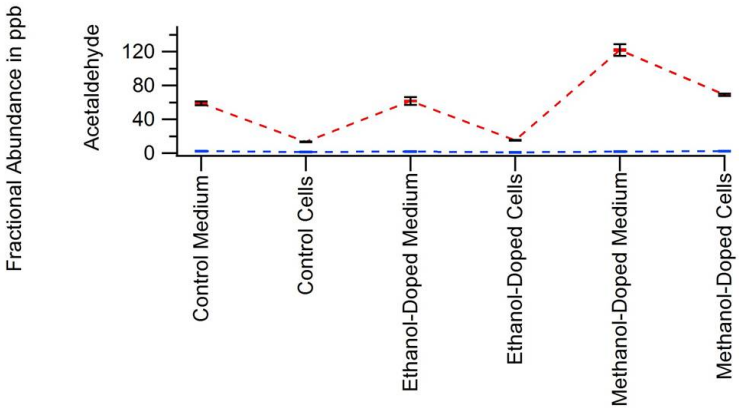

(B)

Figure 4.9: (A) Detected dilutions in parts per billion of formaldehyde, methanol, ethanol, acetone, and acetaldehyde in the second series of Calu-3 medium and cells. Samples analyzed consisted of control medium, control cells, ethanol-doped medium, ethanol-doped cells, methanol-doped medium, methanol-doped cells, acetaldehyde-doped medium, and acetaldehyde-doped cells. (B) Detected dilutions in parts per billion of acetaldehyde in the second series of Calu-3 medium and cells for the control medium, control cells, ethanol-doped medium, ethanol-doped cells, methanol-doped medium, and methanol-doped cells.

Similar trends were observed in the primary epithelial airway cells for the second series, as illustrated in Figure 4.10. Formaldehyde was below the contamination threshold for all samples. For non-doped cases, methanol was consistently close to 50 ppb. Interestingly, methanol levels increased in the doped cell collection, jumping from 700 ppb in the medium to 900 ppb in the presence of cells. Despite increasing the doping level from 5 ppm to 10 ppm, the increase in ethanol was still smaller than anticipated. In the second series of primary airway cells, ethanol behaved opposite to acetaldehyde. Concentrations were higher in the cells than in medium. The approximate changes in dilution were as follows: 100 ppb in the control group, 200 ppb in the ethanol doping cases, 500 ppb in the methanol doping cases, and 100 ppb in the acetaldehyde doping cases. Acetone was only marginally above baseline except for the methanol-doped cells collection, where it was approximately 50 ppb higher. Acetaldehyde levels were higher in the medium than with the cells. For the cases in which medium was not doped with acetaldehyde, acetaldehyde dilutions are near baseline when cells are present. Changes between medium and cells range from 40 to 60 ppb in the non-acetaldehyde-doped cases. Acetaldehyde levels did not return to baseline in the cell sample when doped with acetaldehyde. In the medium, acetaldehyde was present in roughly 1000 ppb, and was reduced to approximately 300 ppb in the presence of cells, a change of 700 ppb.

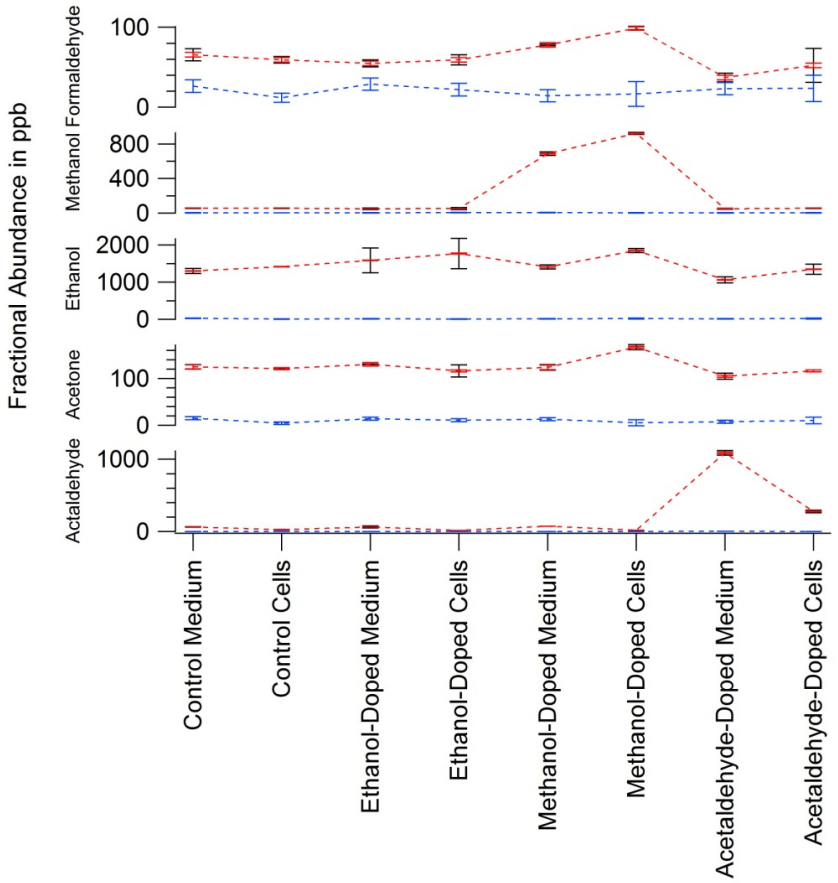

(A)

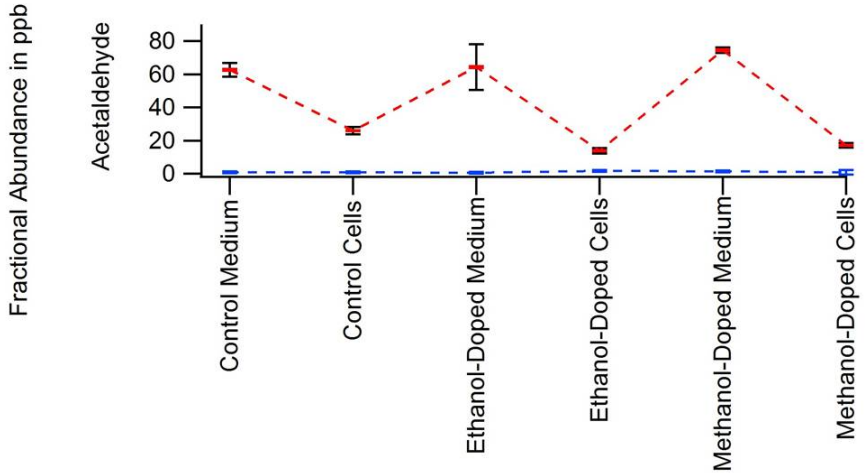

(B)

Figure 4.10: (A) Detected dilutions in parts per billion of formaldehyde, methanol, ethanol, acetone, and acetaldehyde in the second series of primary epithelial airway medium and cells. Samples analyzed consisted of control medium, control cells, ethanol-doped medium, ethanol-doped cells, methanol-doped medium, methanol-doped cells, acetaldehyde-doped medium, and acetaldehyde-doped cells. (B) Detected dilutions in parts per billion of acetaldehyde in the second series of primary epithelial airway medium and cells for the control medium, control cells, ethanol-doped medium, ethanol-doped cells, methanol-doped medium, and methanol-doped cells.

A second series was also conducted in Hep G2 cells. Figure 4.11 shows the data for this second series. Formaldehyde levels were below the contamination threshold across all samples. Methanol levels were above baseline in all collections, and were consistently near 50 ppb in non-methanol-doped collections. Unlike in the first series of Hep G2 collections, methanol increased between methanol-doped medium and methanol-doped cells. A difference of approximately 100 ppb was observed between medium and cells in the case of methanol doping. Ethanol dilutions were above the contamination limit in all samples but the acetaldehyde-doped cells. Ethanol dilutions increased between medium and cells in the control and methanol-doped cases. There was a decrease in dilution between the medium and cells in the ethanol-doped and acetaldehyde-doped cases. The most significant change in ethanol was a decrease from approximately 500 ppb in the acetaldehyde-doped medium to approximately 100 ppb in the acetaldehyde-doped cell collection. Acetone was consistently below the contamination limit for these collections. Acetaldehyde levels followed the previously observed pattern of decrease in the presence of cells. Contrary to the other series of collections, however, acetaldehyde dilutions were nearly identical across medium samples, near 50 ppb, and across cell samples, near the baseline, except for the case of acetaldehyde doping. Acetaldehyde dilutions dropped from approximately 1500 ppb in the doped medium to approximately 100 ppb in the doped cells.

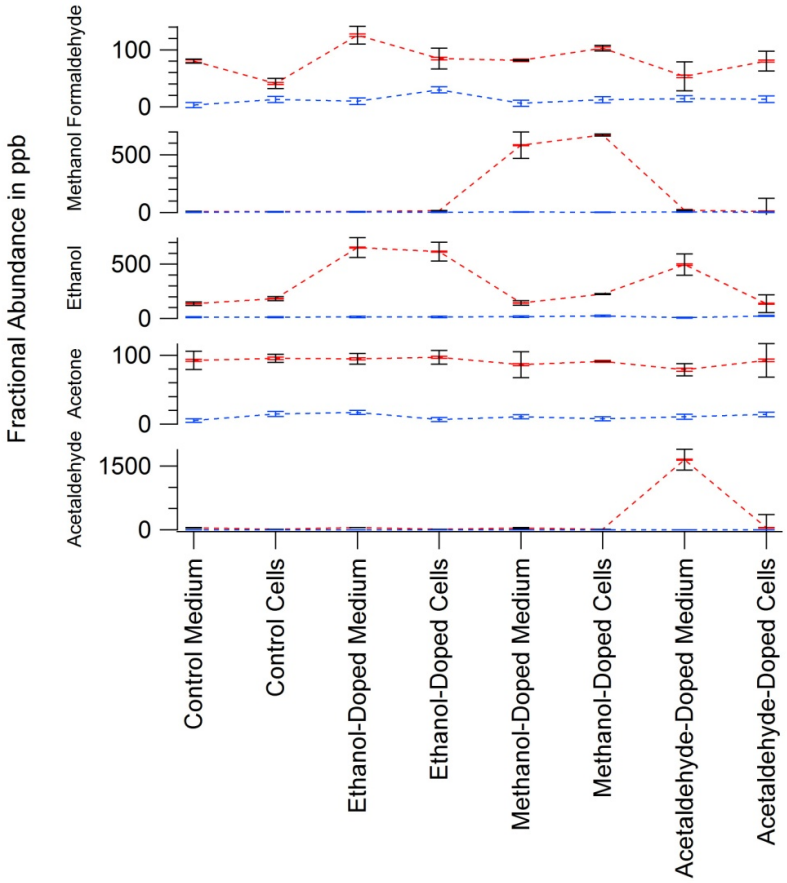

(A)

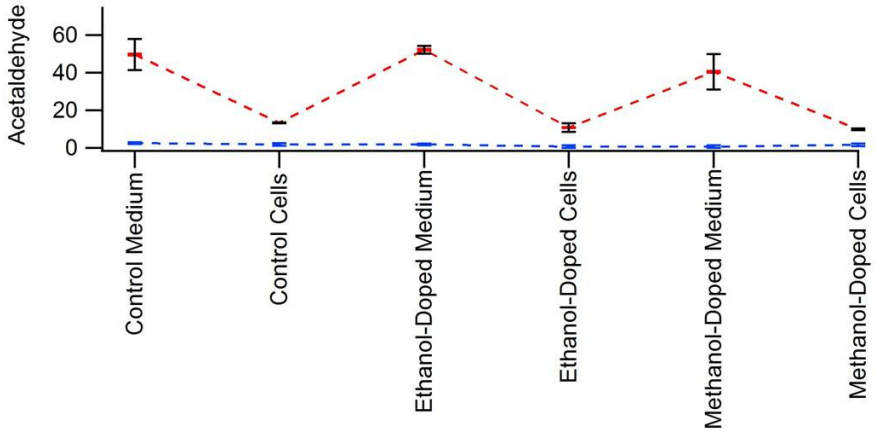

(B)

Figure 4.11: (A) Detected dilutions in parts per billion of formaldehyde, methanol, ethanol, acetone, and acetaldehyde in the second series of Hep G2 medium and cells. Samples analyzed consisted of control medium, control cells, ethanol-doped medium, ethanol-doped cells, methanol-doped medium, methanol-doped cells, acetaldehyde-doped medium, and acetaldehyde-doped cells. (B) Detected dilutions in parts per billion of acetaldehyde in the second series of Hep G2 medium and cells for the control medium, control cells, ethanol-doped medium, ethanol-doped cells, methanol-doped medium, and methanol-doped cells.

4.1.7 Metabolic Changes in Response to Altered Glucose Transport

In order to probe the metabolic response of the cells in response to altered glucose transport into cells, special media were prepared with low glucose and no insulin, respectively. Primary cells were selected for this test due to the ability to modulate glucose and insulin content in the medium. Collections were made over a period of five hours. One sample was collected from 0 to 2.5 hours and a second from 2.5 to 5 hours. Figure 4.12 depicts the data for the control group. Figure 4.13 portrays the trends in a low

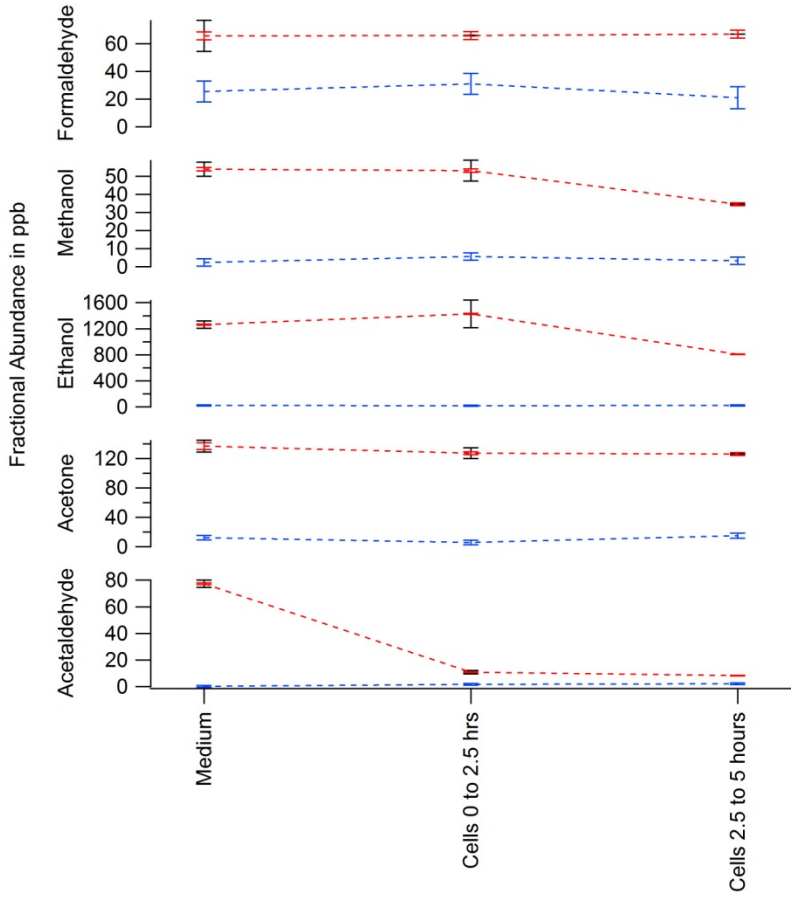

Figure 4.12: Detected dilutions in parts per billion of formaldehyde, methanol, ethanol, acetone, and acetaldehyde in control medium and cells. Medium was collected once for 2.5 hours. 2 bags were collected for cells: one from 0 to 2.5 hours and one from 2.5 to 5 hours.

glucose environment. Figure 4.14 shows the data for medium and cells in the absence of insulin. Formaldehyde levels were below the contamination threshold in all samples.

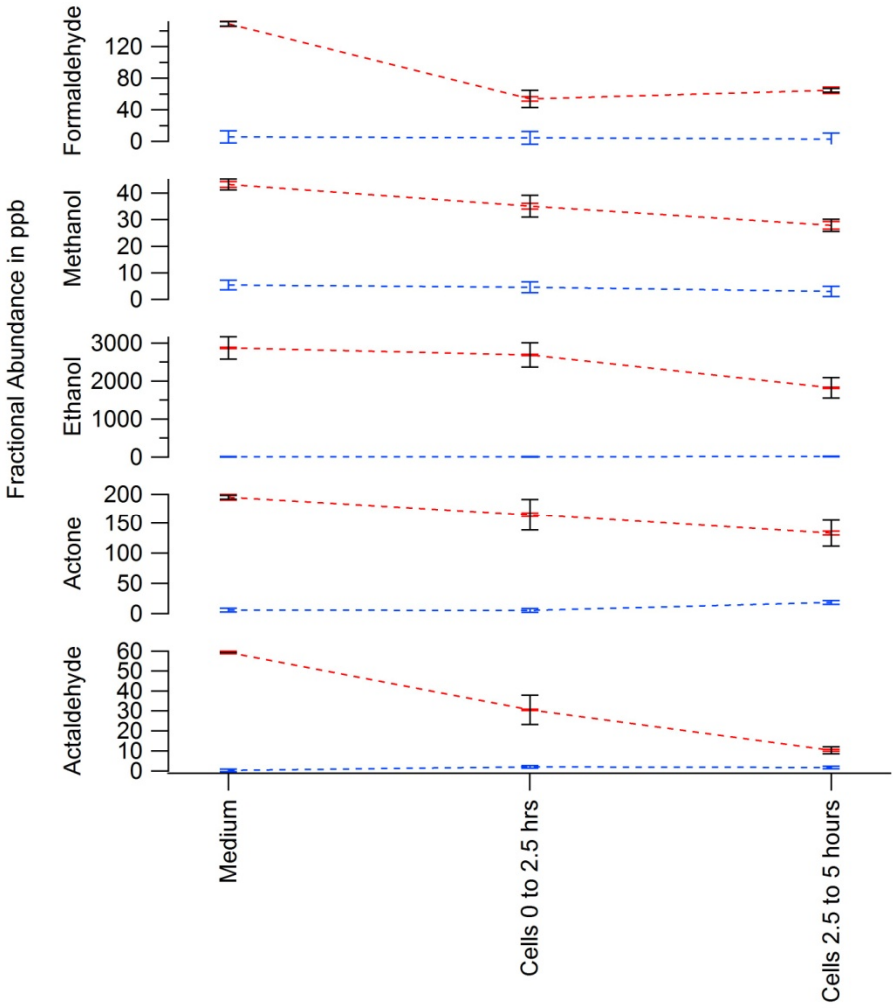

Figure 4.13: Detected dilutions in parts per billion of formaldehyde, methanol, ethanol, acetone, and acetaldehyde in low glucose medium and cells. Medium was collected once for 2.5 hours. 2 bags were collected for cells: one from 0 to 2.5 hours and one from 2.5 to 5 hours.

Methanol was above baseline in all collections. In the control collections, methanol was near 50 ppb in the medium and in the 0 to 2.5 hour collections, dropping to roughly 30 ppb in the 2.5 to 5 hour collection. In the low glucose environment, there was a steady decline of approximately 5 ppb in methanol from one sample to the next, starting at approximately 40 ppb and ending near 30 ppb. Methanol levels varied only slightly in the samples with an absence of insulin. Ethanol was above the contamination limit in all collections. For the control group, ethanol dilution was approximately 1200 ppb in the

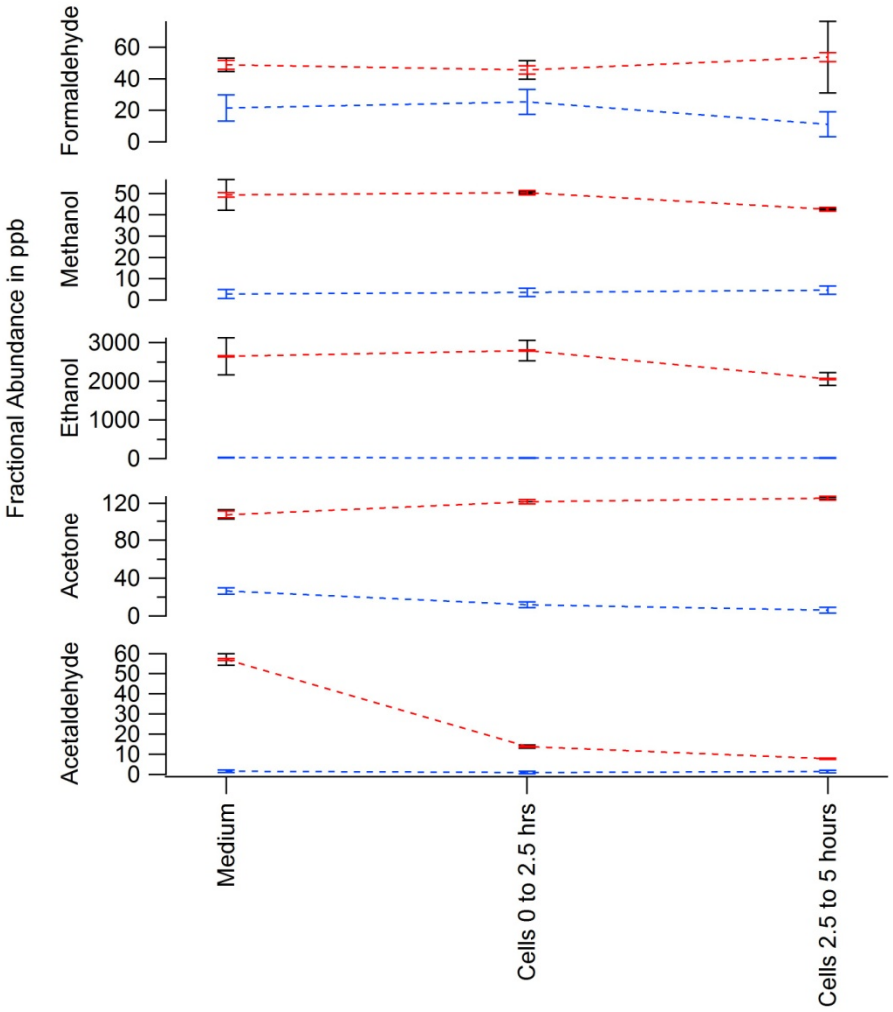

Figure 4.14: Detected dilutions in parts per billion of formaldehyde, methanol, ethanol, acetone, and acetaldehyde in medium and cells with no insulin. Medium was collected once for 2.5 hours. 2 bags were collected for cells: one from 0 to 2.5 hours and one from 2.5 to 5 hours.

medium, increased to 1400ppb in the first 2.5 hours, and decreased to 1000 ppb in the second 2.5 hours. For the low glucose environment, ethanol dilution started near 2800 ppb in the medium, fell to approximately 2700 ppb in the first 2.5 hours, then fell to approximately 2000 ppb in the second 2.5 hours. In the absence of insulin, the ethanol levels varied from 2600 ppb in the medium to 2900 ppb in the first 2.5 hours, to 2100 ppb in the second 2.5 hours. In the control environment, acetone was relatively consistent, staying between roughly 120 ppb and 130 ppb. In the low glucose environment, acetone

levels decreased by approximately 25 ppb for each 2.5 hours, starting at 200 ppb in the medium and dropping to 150 after the second 2.5 hours. In the absence of insulin, acetaldehyde levels demonstrated a small but statistically determined increase, in a alignment with the anticipated behavior. Acetaldehyde concentration started at roughly 80 ppb in the control medium and dropped to baseline for the subsequent runs with cells. Similar behavior was observed in the absence of insulin, starting at 60 ppb instead of 80 ppb. For the low glucose environment, acetaldehyde appears to have been metabolized more slowly by the cells. Dilutions dropped from approximately 60 ppb in the medium to 30 ppb in the first 2.5 hours, then dropped to near baseline in the second 2.5 hours.

4.1.8 Experimental Determination of the Rates of Acetaldehyde Consumption

The most prominent and statistically determined result of the experiments described in this thesis was the difference in gaseous acetaldehyde between medium and cells. The THz gas sensor allows for the calculation of the consumption rates of key analytes. Rates of acetaldehyde consumption were calculated for each cell type according to following equation:

$$R = \frac{N_{Consumed}}{N_{Cells} * t}$$

Eq. 4.1

where R is the rate of acetaldehyde consumption in units of molecules s^{-1} $cell^{-1}$, t is the collection time in seconds, N_{Cells} is the number of cells in the culture as listed in Table 4.1[2], and $N_{Consumed}$ is the number of molecules of acetaldehyde consumed, calculated as:

[2] Cell counts are estimates. Three of the 24 wells were selected and the number of cells in each was counted. This number was then averaged and multiplied by 24 to attain an approximate total cell count.

$$N_{Consumed} = \frac{\Delta\, p\, V}{a\, k\, T}$$

Eq. 4.2

where Δ is the difference in dilution between acetaldehyde-doped medium and acetaldehyde-doped cells, p is the pressure of the gas (101325 Pa), V is the volume collected, a is the preconcentrator efficiency (63.4% for acetaldehyde as depicted in Table 3.1), k is Boltzmann's constant, and T is the temperature of collection in Kelvin.

Cell Type	Number of Cells
Calu-3	6.67 10^6
Primary Epithelial Airway	1.83 10^7
Hep G2	1.48 10^7

Table 4.1: Cell counts used in calculating rate of acetaldehyde consumption for each type of cell.

Figure 4.15 shows the datasets used in these calculations, consisting of acetaldehyde dilutions in medium and cells for each cell type. In Calu-3 cells, the rate of consumption was 9.87 x 10^5 molecules $cell^{-1}$ s^{-1}. Rate of consumption in primary epithelial airway cells was 5.99 x 10^5. In Hep G2 cells, the rate of consumption of acetaldehyde was 4.83 x 10^5 molecules $cell^{-1}$ s^{-1}. Figure 4.16 displays these numbers graphically.

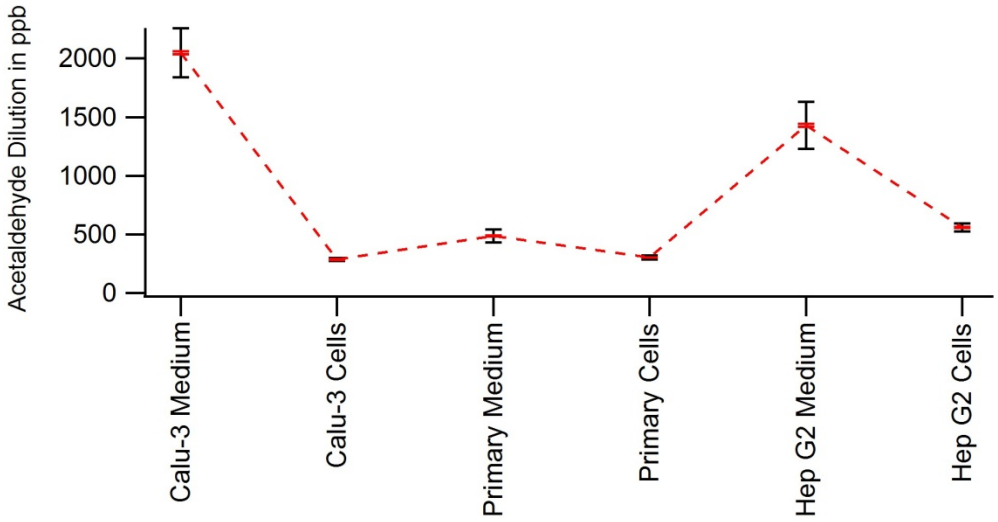

Figure 4.15: Detected dilution of acetaldehyde. Samples were collected in Calu-3 medium and cells, primary epithelial airway medium and cells, and Hep G2 medium and cells.

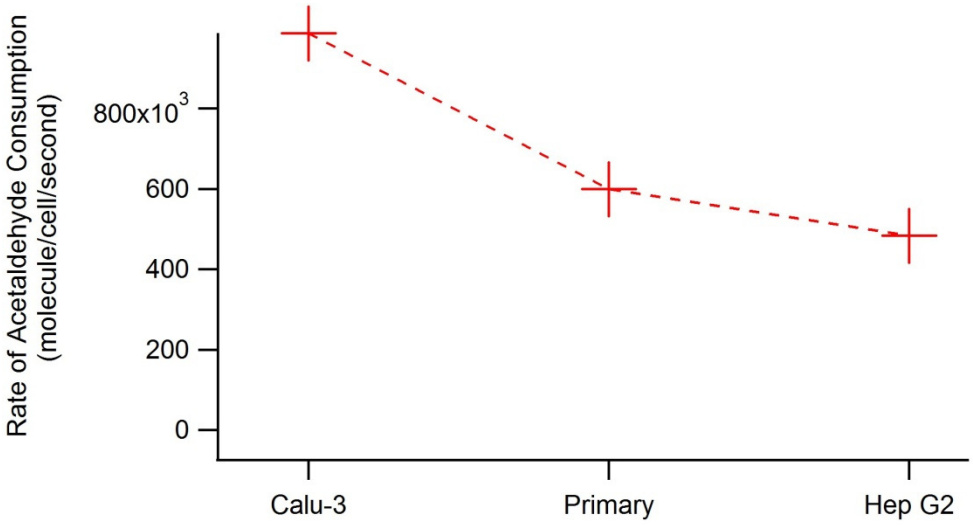

Figure 4.16: Rate of consumption of acetaldehyde in molecules per cell per second. Rates were calculated for each cell type: Calu-3 cells, primary epithelial airway cells, and Hep G2 cells.

In order to determine repeatability of these measurements, the same calculation was made for three analogous pairs of samples in Hep G2 medium and cells. Figure 4.17 shows the dilutions for each sample. Figure 4.18 shows the calculated rates for each. The

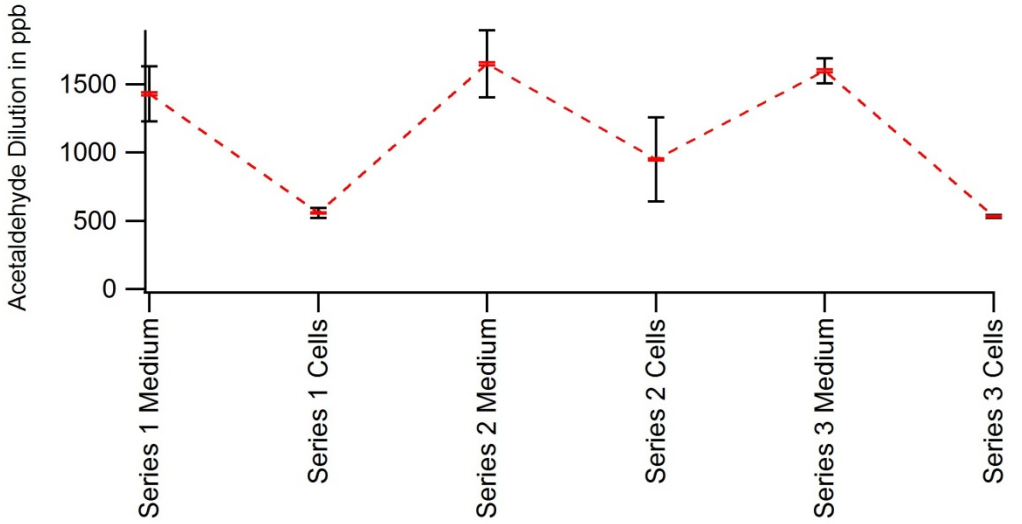

Figure 4.17: Detected dilution of acetaldehyde. Samples were collected in pairs of medium and cells for three individual sets of cells. Each was doped with acetaldehyde.

fourth data point in Figure 4.18 corresponds to the average value.

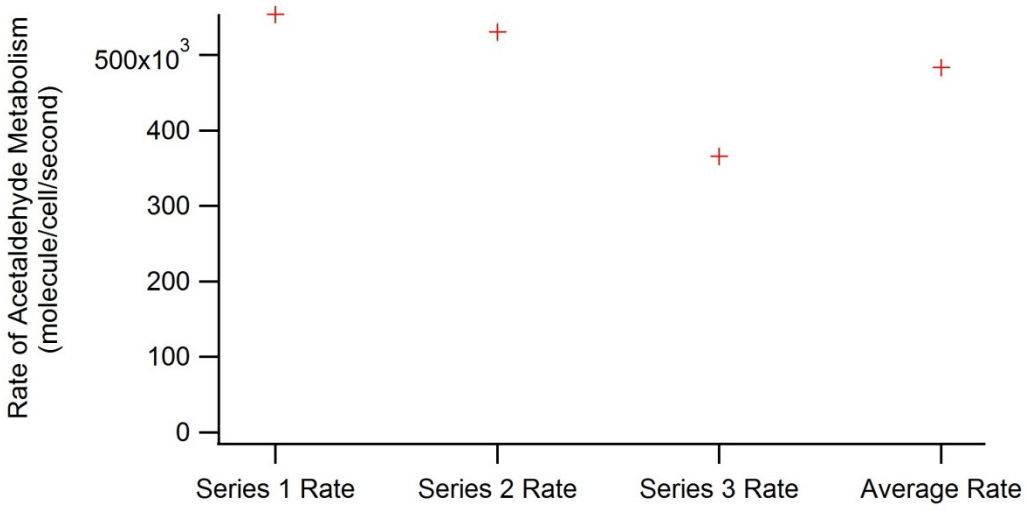

Figure 4.18: Rates of acetaldehyde consumption for each series of Hep G2 and the average rate.

Chapter 5

5.1 Discussion and Conclusions

Throughout the experiments, formaldehyde was detected above chemical background in the spectroscopic chamber, indicating formaldehyde was present in the collected gaseous samples. Formaldehyde was below the contamination threshold determined from the background of various components of the collection system. The most likely source of the formaldehyde in the experiments was the cell enclosure

Trends in methanol were not consistent in the doping collection series, even within the same cell type. For the first series of Calu-3 the anticipated decrease between medium and cells was observed. However, for the second series the dilution was nearly unchanged between medium and cells. No significant change of gaseous methanol was observed in the methanol-doped series of primary airway cells. In the second series of primary airway cells and both series of Hep G2 cells, there was actually an increase in methanol between medium and cells. Due to the lack of consistent trends in methanol dilutions in the case of doping, no conclusions are drawn at this time about methanol metabolism of the cells. Results of testing in environments with low glucose and without insulin provided more fruitful results. In both the control and no insulin environments, cells slightly reduced methanol in the first 2.5 hours when compared with medium, and then dramatically reduced methanol in the second 2.5 hours. In the low glucose environment, methanol dropped nearly linearly, indicating a more steady metabolism of methanol by the cells. It is clear from these results that under normal conditions, 2.5 hours is insufficient time to observe a significant change in methanol. By extending

collection times or by allowing cells to be in methanol-doped medium prior to collecting, consistent results in methanol may be observed.

Ethanol levels did not show any statistically determined trends in the doping series. In Calu-3 cells, ethanol often increased slightly between medium and cells in the non-ethanol-doped cases. For the ethanol-doped collections ethanol decreased slightly from medium to cells or remained approximately equal. In the primary epithelial airway cells, slight increases between medium and cells were observed for all samples. In Hep G2 cells, behavior was not consistent between series for methanol doping. A slight increase between medium and cells was observed for both series in the control group. Slight decreases in ethanol dilutions were recorded when doped with ethanol in both series. Decreases in ethanol between medium and cells doped with acetaldehyde were consistent across both series. As can be seen from the standard deviations in the Figures 4.1-4.14, there was somewhat high inconsistency in measured ethanol dilutions, even between samples drawn from the same collection bag. It is believed this is variation arises from inconsistency of the preconcentrator in trapping ethanol. In testing low glucose and no insulin environments, like with methanol, ethanol behavior was similar between control and no insulin environments. For each, a slight increase was observed between medium and cells for the first 2.5 hours. In the low glucose environment, a small decrease was observed between medium and the first 2.5 hours in cells. For all three environments, a large decrease in ethanol was observed between 2.5 and 5 hours, further supporting the hypothesis that the 2.5 hour collection window for most of the collections made was too small to observe significant changes in ethanol.

Acetone did not exhibit any statistically determined variance across the doping series. Acetone was included in this study to probe potential changes in metabolism when cell glucose was depleted. It is unlikely that cells appreciably depleted glucose in the medium within the 2.5 collection window of the doping series. Under these considerations, the relative stability of acetone dilutions is an expected result. In testing the cells in environments of low glucose and the absence of insulin, as before, control cells did not demonstrate a statistically determined difference in acetone levels. The acetone profile was relatively flat and close to baseline. As insulin and glucose levels were not altered, this behavior was expected in the control group. For the low glucose environment, acetone was detected in greater quantities in both medium and cells. Acetone showed a steady, nearly linear decline in the subsequent collections with cells. However, when cells were not provided with insulin, acetone levels demonstrated a small but statistically determined increase. From prior research, it was anticipated that acetone would increase as glucose decreased. [27] As mentioned, it is unlikely that the cells entirely depleted the glucose, and so it is not surprising that acetone did not increase in the low glucose environment. Acetone appears to have been produced when no insulin was supplied to the cells, which agrees with predicted behavior. As with methanol and ethanol metabolism, extending the duration of collection may produce a different result and would be a good avenue for further investigation.

Trends in acetaldehyde dilutions were consistent across all three cell types. Acetaldehyde dilutions dropped significantly between medium and corresponding cell collections. Though general behavior was the same across each type of cell, rates of metabolism differed between cell types. Calu-3 cells converted acetaldehyde at a rate of

9.87 x 10^5 molecules $cell^{-1}$ s^{-1}. Rate of consumption in primary epithelial airway cells was 5.99 x 10^5. The rate at which acetaldehyde was metabolized by Hep G2 cells was 4.83 x 10^5 molecules $cell^{-1}$ s^{-1}. Acetaldehyde was processed nearly twice as fast in Calu-3 cells as in Hep G2 cells. This points to more metabolic efficiency in lung cells as opposed to liver cells. It should be noted, however, that both lines are cancerous. Further study is needed involving primary lung and primary liver cell lines to determine whether this behavior is observed in healthy cells from these tissues. Calu-3 cells metabolized acetaldehyde at a rate nearly double that of healthy lung cells. This behavior may be a result of the fact that Calu-3 cells are able to use acetaldehyde as an alternate energy source. [30] Primary lung cells metabolized acetaldehyde at a faster rate than did Hep G2 cells. At first glance, this is an alarming result, considering most alcohol and aldehyde metabolism occurs in the liver. However, these are cancerous liver cells and studies have shown that the enzymes responsible for metabolism of ethanol and acetaldehyde are downregulated in Hep G2 cells as compared with healthy liver cells. [27] The above results indicate that cells are able to metabolize acetaldehyde on the time scale of the experiment, but are not able to metabolize ethanol or methanol. A question then arises if the reduction in acetaldehyde is caused by dehydrogenase enzymes on the associated timescale. A possible alternative are the antioxidants present in these cells. These antioxidants are present to prevent the destruction of cell barriers by reactive oxygen species such as acetaldehyde. It is possible that these antioxidants act on a much faster time scale than the enzymes, leading to the observed behavior in acetaldehyde, but not in ethanol or methanol. Antioxidants naturally exist in abundance in lung tissue, which is regularly bombarded by reactive oxygen species from inhaled air. The liver, on the other

hand, is not exposed to these agents in such great quantities and contains less antioxidants. Were this the case, it would explain the nearly double rate of acetaldehyde metabolism in lung cell cultures. Another possible explanation for this difference in consumption rate between Calu-3 cells and Hep G2 cells is the absence or downregulation of dehydrogenase enzymes in Hep G2 cells. [17] Regardless of the underlying cause, based on the results of this study, cell culture types appear to be distinguishable by the rate at which they process acetaldehyde. It has been shown that cancerous lung cells consume acetaldehyde at nearly double the rate of healthy lung cells. Further, cancerous liver cells metabolized acetaldehyde the most slowly of the cell types under investigation.

One particular challenge of the study was assuring contamination did not impact results. As discussed before, a contamination baseline was established in order to assess whether detected dilutions were significant or due to contamination. Bags used in the study were recycled from previous work. Each bag was purged before and after each run to minimize residual contamination. However, because the system is sensitive to even trace dilutions, even minimal contamination influence detected dilutions.

Another challenge of the study was the fact that cells were submerged in medium. As gas was passed above each well in the enclosure, only those VOCs that evolved from solution were collected. Therefore any compounds of interest that remained in solution were not detected.

Finally, cells used in these experiments were in culture. It has not been determined whether metabolic behavior of cells in culture is analogous to that of cells in

the body. In particular, liver cells are cultured in a monolayer. In the body, liver cells are found in clusters, surrounded by blood vessels.

Improvements to the experiment are planned including upgrades to the collection system. In the present setup, cells are submerged beneath media in each well of a 24-well plate. As such, only those analytes that have evolved out of the solution are collected. A future design involves a configuration with cells sitting at the air-liquid interface in the medium, as in Figure 3.4(a). In this configuration, more VOCs may be detected, including acetic acid and formic acid. Both acetic acid and formic acid have spectral lines within the range of the spectrometer. In fact, lines of each have been detected, but were not included in the experiments in this thesis. Figure 5.1 shows the detected formic acid spectral feature with line center frequency at 262.1036304 GHz. In addition, plans are in

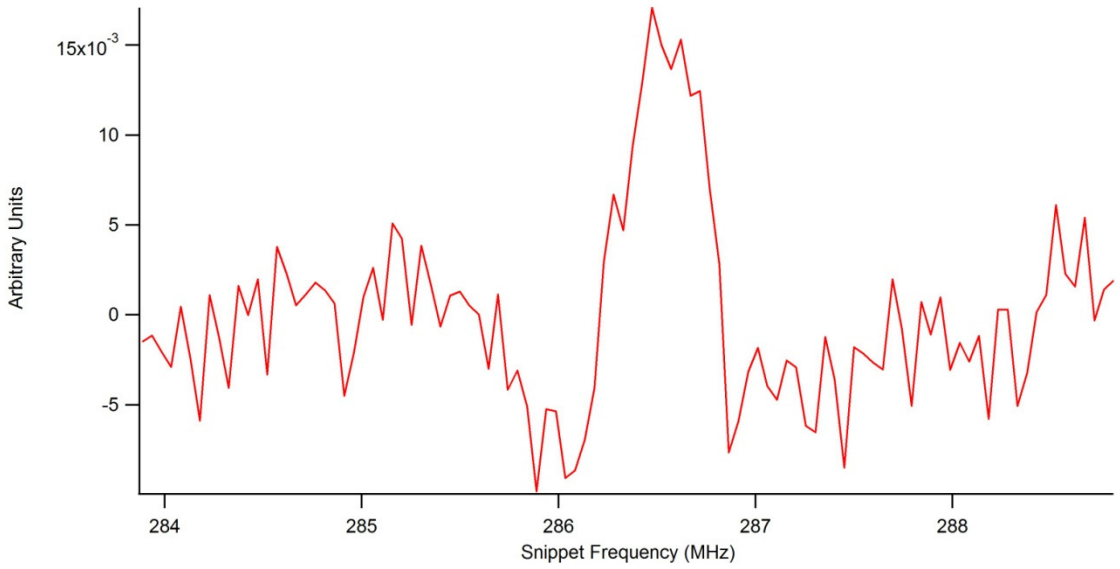

Figure 5.1: Detected spectral line of formic acid.

place to test primary liver cells. Doing so will serve both as a point of comparison with primary airway cells and as a point of comparison with cancerous liver cells. The

addition of primary liver cells will allow for a more complete comparison between healthy and cancerous cell lines as well as between lung and liver tissues.

It has been shown that cells can be differentiated by the rate at which they metabolize acetaldehyde. With the improvements discussed, this same diagnostic could be extended to other VOCs. Differences between cell types has been established, but this same diagnostic could also be applied to variations in the same cell. For instance, metabolic rates could be compared between healthy cells and those with bacterial or viral infections. Provided that patterns establish differences between metabolic rates of healthy and cancerous cells across multiple cancerous and primary cell lines, this technique could be applied to early detection and diagnosis of cancer in lung cells.

The aim of this study was to develop a novel technique for probing metabolic processes in cell cultures. THz rotational spectroscopy has not previously been used to evaluate gaseous emissions of cell cultures. Cell cultures from both primary and immortal lung cell lines as well as an immortal liver cell line were investigated. Cells were doped with various agents to investigate the metabolic rates of consumption for these agents.

Viability of THz rotational spectroscopy as a means of identifying cell cultures through changes in acetaldehyde dilutions was established. With further study, other compounds will be incorporated for use in this technique. Future work could also extend this application to other realms of study, including differentiation between healthy and diabetic cells or between healthy cells and those with viral or bacterial infections. In addition, with further study, it may be possible to compare the metabolic activity of cells in cultures to breath from living subjects. Establishing this link would provide the means

for an entirely new branch of biological and medical research using THz rotational spectroscopy.

Appendix 1

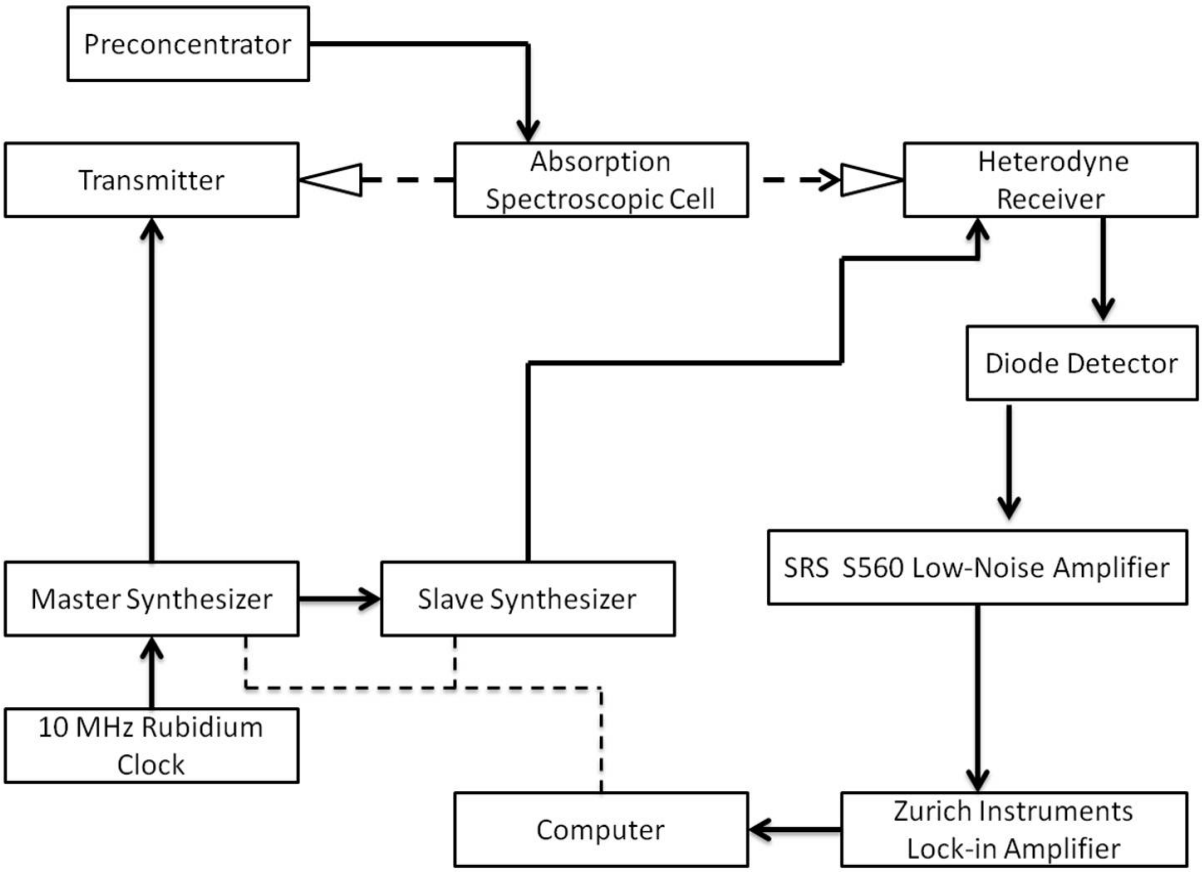

Figure A.1: Schematic layout of the spectroscopic system used. This schematic was adapted from previously published worked. [9][27]

Appendix 2

The media used in this study were prepared according to standard guidelines. It is important to note the ingredients in each of these media, as some of them may play a role in the spectra that are collected. Table A.1 shows the components of the medium used in conjunction with the Calu-3 cells. RPMI stands for Roswell Park Memorial Institute Medium. Table A.2 contains the components of RPMI. FBS stands for fetal bovine serum, used for proteins and growth factors. Finally penicillin streptomycin is used as an antibiotic to prevent the growth of bacteria in the medium.

Substance	Quantity	Purpose
RPMI	50 ml	Growth Medium
FBS	5 ml	
Penicillin streptomycin	.55 ml	Anitibiotics

Table A.1: Calu-3 complete medium components.

Formulation for RPMI-1640 Medium			
Inorganic Salts (g/liter)		**Vitamins (g/liter)**	
$Ca(NO_3)_2 \cdot 4H_2O$	0.10000	D-Biotin	0.00020
$MgSO_4$ (anhydrous)	0.04884	Choline Chloride	0.00300
KCl	0.40000	Folic Acid	0.00100
$NaHCO_3$	1.50000	myo-Inositol	0.03500
NaCl	6.00000	Nicotinamide	0.00100
Na_2HPO_4 (anhydrous)	0.80000	p-Amino Benzoic Acid	0.00100
		D-Pantothenic Acid (hemicalcium)	0.00025
Amino Acids (g/liter)		Pyridoxine·HCl	0.00100
L-Arginine (free base)	0.20000	Riboflavin	0.00020
L-Asparagine·H_2O	0.05682	Thiamine·HCl	0.00100
L-Aspartic Acid	0.02000	Vitamin B-12	0.00001
L-Cystine·2HCl	0.06520		
L-Glutamic Acid	0.02000	**Other (g/liter)**	
L-Glutamine	0.30000	D-Glucose	4.50000
Glycine	0.01000	Glutathione (reduced)	0.00100
L-Histidine (free base)	0.01500	HEPES	2.38300
Hydroxy-L-Proline	0.02000	Phenol Red, Sodium Salt	0.00500
L-Isoleucine	0.05000	Sodium Pyruvate	0.11000
L-Leucine	0.05000		
L-Lysine·HCl	0.04000		
L-Methionine	0.01500		
L-Phenylalanine	0.01500		
L-Proline	0.02000		
L-Serine	0.03000		
L-Threonine	0.02000		
L-Tryptophan	0.00500		
L-Tyrosine·2Na·$2H_2O$	0.02883		
L-Valine	0.02000		

Table A.2: Contents of RPMI medium according to ATCC. [31]

Primary cells do not grow in culture as easily as cancerous cells do. Primary cells require a more complex medium. The first component of the total medium used with primary cells is itself a type of medium, called primary complete medium. Table A.3 is comprised of the components of the primary complete medium. Primary complete medium consists of Dulbecco's Modified Eagle's medium, FBS, glutamine, and penicillin streptomycin. Table A.4 contains a detailed list of the components of DMEM. The total

Substance	Quantity	Purpose
DMEM high glucose	50 ml	
FBS	5 ml	
Glutamine	.55 ml	Essential amino acid
Penicillin streptomycin	.55 ml	Anitibiotics

Table A.3: Primary complete medium components.

Formulation for Dulbecco's Modified Eagle's Medium (DMEM)			
Inorganic Salts (g/liter)		**Vitamins (g/liter)**	
$CaCl_2$ (anhydrous)	0.20000	Choline Chloride	0.00400
$Fe(NO_3)_3 \cdot 9H_2O$	0.00010	Folic Acid	0.00400
$MgSO_4$ (anhydrous)	0.09770	myo-Inositol	0.00720
KCl	0.40000	Nicotinamide	0.00400
$NaHCO_3$	1.50000	D-Pantothenic Acid	0.00400
NaCl	6.40000	(hemicalcium)	
$NaH_2PO_4 \cdot H_2O$	0.12500	Pyridoxine·HCl	0.00400
		Riboflavin	0.00040
Amino Acids (g/liter)		Thiamine·HCl	0.00400
L-Arginine·HCl	0.08400		
L-Cystine·2HCl	0.06260		
L-Glutamine	0.58400	**Other (g/liter)**	
Glycine	0.03000	D-Glucose	4.50000
L-Histidine·HCl·H_2O	0.04200	Phenol Red, Sodium Salt	0.01500
L-Isoleucine	0.10500	Sodium Pyruvate	0.11000
L-Leucine	0.10500		
L-Lysine·HCl	0.14600		
L-Methionine	0.03000		
L-Phenylalanine	0.06600		
L-Serine	0.04200		
L-Threonine	0.09500		
L-Tryptophan	0.01600		
L-Tyrosine·2Na·$2H_2O$	0.10379		
L-Valine	0.09400		

Table A.4: List of components of DMEM. [32]

medium used with primary epithelial airway cells is called F-Media. Table A.5 lists the components of F-Media. F-12 nutrient mix is a solution that promotes cell growth. Table A.6 details the components of this mixture. Epidermal growth factor is added to promote

cell growth. Hydrocortisone is a steroid and is dissolved in ethanol. Cholera toxin is an important factor in guiding metabolic processes. Rock inhibitor aids in cell division by reverting cells to a stem cell-like state.

Substance	Quantity	Purpose
Primary Complete Medium	37.3 ml	
F-12 Nutrient Mix	12.5 ml	
Epidermal Growth Factor	50 µl	Growth factor
Hydrocortisone*	50 µl	Steroid used for growth
Insulin	50 µl	Regulates glucose consumption
Amphotericin B	50 µl	Antifungal antibiotic
Cholera Toxin	0.43 µl	Helps guide metabolic processes
Rock Inhibitor	10 µl	Aids in cell division

Table A.5: F-Media components.

Formulation for DMEM:F-12 Medium			
Inorganic Salts (g/liter)		**Vitamins (g/liter)**	
$CaCl_2$ (anhydrous)	0.11665	D-Biotin	0.00000365
$CuSO_4$ (anhydrous)	0.0000008	Choline Chloride	0.00898
$Fe(NO_3)_3 \cdot 9H_2O$	0.00005	Folic Acid	0.00265
$FeSO_4 \cdot 7H_2O$	0.000417	myo-Inositol	0.01261
$MgSO_4$ (anhydrous)	0.08495	Niacinamide	0.00202
KCl	0.3118	D-Pantothenic Acid	0.00224
$NaHCO_3$	1.20000	(hemicalcium)	
NaCl	7.00000	Pyridoxine·HCl	0.00203
Na_2HPO_4 (anhydrous)	0.07100	Riboflavin	0.00022
$NaH_2PO_4 \cdot H_2O$	0.06250	Thiamine·HCl	0.00217
$ZnSO_4 \cdot 7H_2O$	0.000432	Vitamin B-12	0.00068
Amino Acids (g/liter)		**Other (g/liter)**	
L-Alanine	0.00445	D-Glucose	3.15100
L-Arginine·HCl	0.14750	HEPES	3.57480
L-Asparagine·H_2O	0.00750	Hypoxanthine	0.00239
L-Aspartic Acid	0.00665	Linoleic Acid	0.000044
L-Cysteine·HCl·H_2O	0.01756	Phenol Red, Sodium Salt	0.00810
L-Cystine·2HCl	0.03129	Putrescine·2HCl	0.00008
L-Glutamic Acid	0.00735	Pyruvic Acid·Na	0.05500
L-Glutamine	0.36510	DL-Thioctic Acid	0.000105
Glycine	0.01875	Thymidine	0.000365
L-Histidine·HCl·H_2O	0.03148		
L-Isoleucine	0.05437		
L-Leucine	0.05895		
L-Lysine·HCl	0.09135		
L-Methionine	0.01724		
L-Phenylalanine	0.03548		
L-Proline	0.01725		
L-Serine	0.02625		
L-Threonine	0.05355		
L-Tryptophan	0.00902		
L-Tyrosine·2Na·$2H_2O$	0.05582		
L-Valine	0.05285		

Table A.6: Components of DMEM/F-12 nutrient mixture. [33]

Components of Hep G2 medium are similar to Calu-3, and are listed in Table A.7. Eagle's Modified Essential Medium is used in place of RPMI. Table A.8 details the ingredients of EMEM. 10% FBS is added to promote growth. Penicillin streptomycin is added as an antibiotic.

Substance	Quantity	Purpose
EMEM	50 ml	
FBS	5 ml	
Penicillin streptomycin	.55 ml	Anitibiotics

Table A.7: Hep G2 complete medium components.

Formulation for Eagle's Minimum Essential Medium (EMEM)			
Inorganic Salts (g/liter)		**Vitamins (g/liter)**	
$CaCl_2$ (anhydrous)	0.20000	Choline Chloride	0.00100
$MgSO_4$ (anhydrous)	0.09767	Folic Acid	0.00100
KCl	0.40000	myo-Inositol	0.00200
$NaHCO_3$	1.50000	Nicotinamide	0.00100
NaCl	6.80000	D-Pantothenic Acid	0.00100
$NaH_2PO_4 \cdot H_2O$	0.14000	(hemicalcium) Pyridoxine·HCl	0.00100
		Riboflavin	0.00010
Amino Acids (g/liter)		Thiamine·HCl	0.00100
L-Alanine	0.00890		
L-Arginine·HCl	0.12640		
L-Asparagine·H_2O	0.01500	**Other (g/liter)**	
L-Aspartic Acid	0.01330	D-Glucose	1.00000
L-Cystine·2HCl	0.03120	Phenol Red, Sodium Salt	0.01000
L-Glutamic Acid	0.01470	Sodium Pyruvate	0.11000
L-Glutamine	0.29200		
Glycine	0.00750		
L-Histidine·HCl·H_2O	0.04190		
L-Isoleucine	0.05250		
L-Leucine	0.05250		
L-Lysine·HCl	0.07250		
L-Methionine	0.01500		
L-Phenylalanine	0.03250		
L-Proline	0.01150		
L-Serine	0.01050		
L-Threonine	0.04760		
L-Tryptophan	0.01000		
L-Tyrosine·2Na·$2H_2O$	.0.5190		
L-Valine	0.04680		

Table A.8: Hep G2 complete medium components. [34]

Appendix 3

Chemical Name	Center Frequency (GHz)
Acetaldehyde	269.8523432
	212.0291805
	269.8061238
	211.984419
	262.9601208
Acetone	269.4312478
	268.3051931
	259.6183698
	267.1829474
	258.4936676
Ethanol	247.9125977
	235.9835255
	242.62588
	242.4757722
	248.5772988
Methanol	252.4857107
	253.2214289
	253.7558751
	252.2528787
	254.423601
Formaldehyde	225.6978516
	211.2115234
	218.2222656
	218.7601563
	218.4757324

Table A.9: List of snippets and center frequency in GHz organized by compound.

Bibliography

1. I.R. Medvedev, R. Schueler, J. Thomas, K. O, H.-J. Nam, N. Sharma, Q. Zhong, D. Lary, and P. Raskin, *Analysis of Exhaled Human Breath via Terahertz Molecular Spectroscopy*, in *IRMMW-THZ 2016, 41st International Conference on Infrared, Millimeter and Terahertz Waves*. 2016: Copenhagen, Denmark.

2. A.M. Fosnight, B.L. Moran, and I.R. Medvedev, "*Chemical analysis of exhaled human breath using a terahertz spectroscopic approach,"* Applied Physics Letters, **103**(13): p. 133703-5, 2013

3. Chen W, Roslund K, Lehto M, et al. Detection of hydrogen cyanide from oral anaerobes by cavity ring down spectroscopy. *Scientific Reports* [serial online]. March 4, 2016;6:22577. Available from: MEDLINE with Full Text, Ipswich, MA. Accessed August 23, 2017.

4. Lu, M., Shen, J., Li, N., Zhang, Y., Zhang, C., Liang, L., & Xu, X. (2006). Detection and identification of illicit drugs using terahertz imaging. *Journal Of Applied Physics*, *100*(10), 103104. doi:10.1063/1.2388041

5. Stoik, C., Bohn, M., & Blackshire, J. (2010). Nondestructive evaluation of aircraft composites using reflective terahertz time domain spectroscopy. NDT and E International, 43(2), 106-115. doi:10.1016/J.NDTEINT.2009.09.005

6. Xiang Yang, Xiang Zhao, Ke Yang, Yueping Liu, et al., Biomedical Applications of Terahertz Spectroscopy and Imaging, *Trends in Biotechnology*, Vol. 34, Iss. 10, October 2016, pp. 810-824. doi:10.1016/J.TIBTECH.2016.04.008

7. Rahman, A., Rahman, A. K., & Rao, B. (2016). Early detection of skin cancer via terahertz spectral profiling and 3D imaging. *Biosensors & Bioelectronics*, *82*64-70. doi:10.1016/j.bios.2016.03.051

8. 7. C.F. Neese, I.R. Medvedev, G.M. Plummer, A.J. Frank, C.D. Ball, and F.C. De Lucia, "*A Compact Submillimeter/Terahertz Gas Sensor with Efficient Gas Collection, Preconcentration, and ppt Sensitivity,"* Sensors Journal, IEEE, **12**(8): p. 2565 - 2574 2012

9. Schueler, R. *Terahertz Spectroscopic Breath Analysis as a Viable Analytical Chemical Sensing Technique.* 2016

10. *Calu-3 ATCC ® HTB-55™ Homo Sapiens Lung Adenocarcinoma;* ATCC, accessed 14 July 2017.

11. Sharma P, Martis P, Excoffon K. Adenovirus transduction: More complicated than receptor expression. *Virology* [serial online]. February 2017;502:144-151.

Available from: MEDLINE with Full Text, Ipswich, MA. Accessed July 14, 2017.

12. Zakhari S. Overview: How Is Alcohol Metabolized by the Body?. *Alcohol Research & Health* [serial online]. December 2006;29(4):245-255. Available from: Academic Search Complete, Ipswich, MA. Accessed June 22, 2017.

13. *Hep G2 ATCC ® HB-8065™ Homo Sapiens Hepatocellular Carcinoma;* ATCC accessed 14 July 2017.

14. Ostrovsky Y. Endogenous ethanol--its metabolic, behavioral and biomedical significance. *Alcohol (Fayetteville, N.Y.)* [serial online]. July 1986;3(4):239-247. Available from: MEDLINE with Full Text, Ipswich, MA. Accessed August 14, 2017.

15. Siddiq T, Richardson P, Mitchell W, Teare J, Preedy V. Ethanol-induced inhibition of ventricular protein synthesis in vivo and the possible role of acetaldehyde. *Cell Biochemistry And Function* [serial online]. March 1993;11(1):45-54. Available from: MEDLINE with Full Text, Ipswich, MA. Accessed August 15, 2017.

16. Danielsson, Olle, et al. Fundamental Molecular Differences Between Alcohol Dehydrogenase Classes. *Proceedings Of The National Academy Of Sciences Of The United States Of America* [serial online]. 1994;(11):4980. Available from: JSTOR Journals, Ipswich, MA. Accessed August 15, 2017.

17. Guo L, Dial S, Ning B, et al. Similarities and Differences in the Expression of Drug-Metabolizing Enzymes between Human Hepatic Cell Lines and Primary Human Hepatocytes. *Drug Metabolism And Disposition* [serial online]. n.d.;39(3):528-538. Available from: Science Citation Index, Ipswich, MA. Accessed July 28, 2017.

18. Maconi E, Griffini A, Cavazzoni V, Aragozzini F. Reduction of acetaldehyde to ethanol by some micro-organisms and its stereospecificity. The Biochemical Journal [serial online]. March 15, 1988;250(3):929-932. Available from: MEDLINE with Full Text, Ipswich, MA. Accessed June 21, 2017.

19. Liesivuori J, Savolainen H. Methanol and formic acid toxicity: biochemical mechanisms. *Pharmacology & Toxicology* [serial online]. September 1991;69(3):157-163. Available from: MEDLINE with Full Text, Ipswich, MA. Accessed August 14, 2017.

20. Friedenson, B. (2011). A common environmental carcinogen unduly affects carriers of cancer mutations: Carriers of genetic mutations in a specific protective response are more susceptible to an environmental carcinogen. Medical Hypotheses, 77(5), 791-797. doi:10.1016/J.MEHY.2011.07.039

21. Tulpule, Ketki et al. Formaldehyde Metabolism and Formaldehyde-Induced Stimulation of Lactate Production and Glutathione Export in Cultured Neurons. *Journal of Neurochemistry* 2013;125 260-272 Accessed June 21, 2017. doi:10.1111/jnc. 12170

22. Brooker, RJ. *Genetics: Analysis and Principles* (4th Edition). McGraw-Hill Science. 2011.

23. MacAllister, S., Choi, J., Dedina, L., & O'Brien, P. (2011). Metabolic mechanisms of methanol/formaldehyde in isolated rat hepatocytes: Carbonyl-metabolizing enzymes versus oxidative stress. Chemico-Biological Interactions, 191(1-3), 308-314. doi:10.1016/J.CBI.2011.01.017

24. Birben E, Sahiner U, Sackesen C, Erzurum S, Kalayci O. Oxidative stress and antioxidant defense. *The World Allergy Organization Journal* [serial online]. January 2012;5(1):9-19. Available from: MEDLINE with Full Text, Ipswich, MA. Accessed August 16, 2017.

25. Berg, JM, Jl Tymoczko, and L Stryer *Biochemistry. 5th Edition.*W.H Freeman. New York. 2002. Chapter 17, The Citric Acid Cycle.

26. Clayton, G. D. and F. E. Clayton (eds.). *Patty's Industrial Hygiene and Toxicology: Volume 2A, 2B, 2C: Toxicology. 3rd ed.* New York: John Wiley Sons, 1981-1982., p. 4908

27. Thomas, J.R. *Assessment of the Applicability of Terahertz Spectroscopic Breath Sensing Towards Monitoring Type 1 Diabetes Mellitus*. 2015

28. Lenz, Anke-Gabriele, et al. "Inflammatory and oxidative stress responses of an alveolar epithelial cell line to airborne zinc oxide nanoparticles at the air-liquid interface: a comparison with conventional, submerged cell-culture conditions." *BioMed Research International*, 2013. *Academic OneFile*, Accessed 1 Aug. 2017.

29. *Igor Pro* WaveMetrics www.wavemetrics.com/products/igorpro/igorpro.htm

30. Kang J, Lee S, Kim S, et al. Aldehyde dehydrogenase is used by cancer cells for energy metabolism. *Experimental & Molecular Medicine* [serial online]. November 25, 2016;48(11):e272. Available from: MEDLINE with Full Text, Ipswich, MA. Accessed August 16, 2017.

31. *Formulation for RPMI-160 Medium ATCC ® 30-2001;* ATCC, accessed 27 July 2017.

32. *Formulation for Dulbecco's Modified Eagle's Medium (DMEM) ATCC ® 30-2002;* ATCC, accessed 27 July 2017.

33. *Formulation for DMEM:F-12 Medium ATCC ® 30-2006;* ATCC, accessed 27 July 2017.

34. *Formulation for Eagle's Minimum Essential Medium (EMEM) ATCC ® 30-2003;* ATCC, accessed 27 July 2017.